DESIGN OF AN OPTIMAL SLIDING MODE CONTROLLER FOR AN ACTIVE SUSPENSION CONSIDERING NON-LINEAR QUARTER CAR MODEL

A THESIS SUBMITTED TO
THE GRADUATE SCHOOL OF NATURAL AND APPLIED SCIENCES
OF
MIDDLE EAST TECHNICAL UNIVERSITY

BY

FARSHID SADEGHI-KHANEGHAH

IN PARTIAL FULFILLMENT OF THE REQUIREMENTS
FOR
THE DEGREE OF MASTER OF SCIENCE
IN
MECHANICAL ENGINEERING

AUGUST, 2020

Approval of the thesis:

DESIGN OF AN OPTIMAL SLIDING MODE CONTROLLER FOR AN ACTIVE SUSPENSION CONSIDERING NON-LINEAR QUARTER CAR MODEL

submitted by **FARSHID SADEGHI-KHANEGHAH** in partial fulfillment of the requirements for the degree of **Master of Science in Mechanical Engineering Department, Middle East Technical University** by,

Prof. Dr. Halil Kalıpçılar
Dean, Graduate School of **Natural and Applied Sciences** _____

Prof. Dr. Sahir Arıkan
Head of Department, **Mechanical Engineering** _____

Assist. Prof. Dr. Kerem Bayar
Supervisor, **Mechanical Engineering, METU** _____

Examining Committee Members:

Prof. Dr. Ender Ciğeroğlu
Mechanical Engineering, METU _____

Assist. Prof. Dr. Kerem Bayar
Mechanical Engineering, METU _____

Assist. Prof. Dr. Ali Emre Turgut
Mechanical Engineering, METU _____

Assoc. Prof. Dr. Yiğit Yazıcıoğlu
Mechanical Engineering, METU _____

Assoc. Prof. Dr. Can Ulaş Doğruer
Mechanical Engineering, Hacettepe University _____

Date:

I hereby declare that all information in this document has been obtained and presented in accordance with academic rules and ethical conduct. I also declare that, as required by these rules and conduct, I have fully cited and referenced all material and results that are not original to this work.

Name, Surname: Farshid Sadeghi-Khaneghah

Signature :

ABSTRACT

DESIGN OF AN OPTIMAL SLIDING MODE CONTROLLER FOR AN ACTIVE SUSPENSION CONSIDERING NON-LINEAR QUARTER CAR MODEL

Sadeghi-Khaneghah, Farshid
M.S., Department of Mechanical Engineering
Supervisor: Assist. Prof. Dr. Kerem Bayar

August, 2020, 86 pages

A non-linear quarter car model is used in this study for developing a control algorithm for an active suspension system. The control method used, is optimal sliding mode control, along with feedback linearization technique for compensating the non-linear aspects of the plant. In addition to the work in recent literature that applies these control methods, estimation of the static suspension deflection, i.e., vehicle sprung mass is performed. Through simulation results, it is shown that correct information of vehicle sprung mass, compared to taking it as a constant parameter in control design, improves the performance of the controller. This information, in turn, reduces the sprung mass acceleration level and enhances ride comfort.

Keywords: Active Suspension, Optimal Sliding Mode Control, Extended Kalman Filter, Non-linear System

ÖZ

BİR AKTİF SÜSPANSİYON İÇİN DOĞRUSAL OLMAYAN ÇEYREK ARAÇ MODELİ KULLANILARAK YAPILAN OPTİMAL KAYMA MODU KONTROLCÜ TASARIMI

Sadeghi-Khaneghah, Farshid
Yüksek Lisans, Makina Mühendisliği Bölümü
Tez Yöneticisi: Dr. Öğr. Üyesi. Kerem Bayar

2020 , 86 sayfa

Bu çalışmada, aktif süspansiyon kontrol algoritması geliştirmek için doğrusal olmayan çeyrek araç modeli kullanılmıştır. Kullanılan kontrol yöntemi geri besleme doğrusallaştırma tekniği ile birlikte optimal kayma modu kontrolüdür. Bu kontrol yöntemlerini uygulayan literatürdeki son çalışmalara ek olarak, statik süspansiyon sıkışmasının, başka bir deyişle aracın yaylanan kütlesinin tahmini de yapılmaktadır. Simülasyon sonuçları aracılığıyla aracın yaylanan kütle bilgisinin, sabit bir parametre olarak alınması yerine kestirilmesinin kontrolcünün performansını geliştirdiği gösterilmiştir. Böylelikle yaylanan kütle ivmesinin düşürüldüğü ve sürüş konforunun iyileştirildiği ortaya koyulmuştur.

Anahtar Kelimeler: Aktif Süspansiyon, Optimal Kayma Modu Kontrolü, Genişletilmiş Kalman Filtresi, Doğrusal Olmayan Sistem

I dedicate this thesis to my brother, who was always supportive of me in my life.

ACKNOWLEDGMENTS

This study was conducted under The Scientific and Technological Research Council of Turkey (Tübitak) project number 218M917.

TABLE OF CONTENTS

LIST OF TABLES

TABLES

LIST OF FIGURES

FIGURES

LIST OF ABBREVIATIONS

ABBREVIATIONS

1D	1 Dimension
2D	2 Dimension
3D	3 Dimension
DOF	Degree of Freedom
QCM	Quarter Car Model
RMS	Root Mean Square
EKF	Extended Kalman Filter
PSD	Power Spectral Density Function
OSMC	Optimal Sliding Mode Control
IOSMC	Improved Optimal Sliding Mode Control
T-S fuzzy	Takagi-Sugeno fuzzy
SMA	Sprung Mass Acceleration
LMI	Linear Matrix Inequality
LQR	Linear Quadratic Regulator

CHAPTER 1

INTRODUCTION

1.1 Motivation and Problem Definition

Ride comfort is among the most important assessment criteria regarding ground vehicles. The responsible part of the vehicle for this matter is the suspension system. Conventional suspension systems are passive suspensions and can improve ride comfort of the vehicle within specified limits. Active suspension systems on the other hand provide a wider ride comfort improvement range.

Nowadays, design of the active suspension and its controller to achieve best ride comfort, is a hot topic in the research field of the vehicle dynamics. Engineers introduce powerful controllers recently.

Designing an effective controller that is robust against road roughness and parameter changes, such as sprung mass, is a crucial need in achieving the best ride comfort.

1.2 Proposed Method

In this study, a controller within the concept of an active suspension system is developed considering non-linear Quarter Car Model. The controller utilizes optimal sliding mode control method. This controller, shows robustness against parameter uncertainties and road roughness.

In addition to the controller, a parameter estimator is developed to estimate the vehicle mass. The estimation method used is the Extended Kalman Filter. The estimation is done for three different cases of vehicle mass.

1.3 Contributions and Novelties

Our contributions are as follows:

- Design of an optimal sliding mode Control for the linearized quarter car model.
- Demonstrating effect of using incorrect vehicle mass in the control algorithm on the performance of the active suspension.

1.4 The Outline of the Thesis

In Chapter 1 motivation and contributions of this work is introduced.

In Chapter 2 A literature review of active suspension controllers and different methods of mitigating the effects of uncertainties are discussed. Also, the advantages of the current study are stated.

In Chapter 3 the mathematical model used for the suspension system and the associated equations of motion are given.

In Chapter 4 the importance of knowing the correct vehicle mass for controller design is explained and an extended Kalman filter is developed for estimating it.

In Chapter 5 the mathematical procedure for deriving the optimal sliding mode controller is given. Also, the method for linearizing the non-linear quarter car model equations is explained.

In Chapter 6 the simulation method, the ISO standards used for representing the road profile and ride comfort, and the parameters used in this study are given.

In Chapter 7 results of the simulations are presented. Then, these results are discussed. Also, possible future work is discussed.

CHAPTER 2

BACKGROUND

2.1 Introduction

In this chapter, ride comfort and different types of suspension systems are described. Then different control methods applied to active suspension systems are mentioned. Usage of optimal sliding mode control in active suspensions and how uncertainties are handled in these systems are explained.

2.2 Ride Comfort

How the passengers of a vehicle are effected by vehicle vibrations, is generally named as ride or ride comfort. A good level of ride comfort, means comfortable ride for passengers. Ride comfort is among the most important assessment criteria regarding ground vehicles. It is generally quantified by the RMS value of the vehicle sprung mass acceleration.

2.3 Suspension Types

The three types of suspension systems in academic and industrial literature, are passive, semi-active and active suspension. All three kinds are discussed in the following sections.

2.3.1 Passive

Conventional suspension systems are passive, and consist of spring and damper elements. This kind of suspension is shown with a simple two DOF model in figure 2.1 part (a). If a soft spring is selected for the passive suspension, the first natural frequency of the suspension, usually called as body bounce frequency which is around 1 Hz, decreases. This improves ride comfort by decreasing sprung mass acceleration in $3 - 9$ Hz frequency range. This frequency range is the important range, for ride comfort of human body [1]. On the other hand it causes a large relative displacement between sprung and unsprung mass. In other words, suspension deflection which is needed to be kept limited, increases. Furthermore, a soft spring causes less force on the tire, which reduces road holding property of the suspension [2]. So, designing of passive suspension is always a trade-off between ride comfort and handling. Semi-active [3] and active suspension systems [4] provide a solution considering this trade-off.

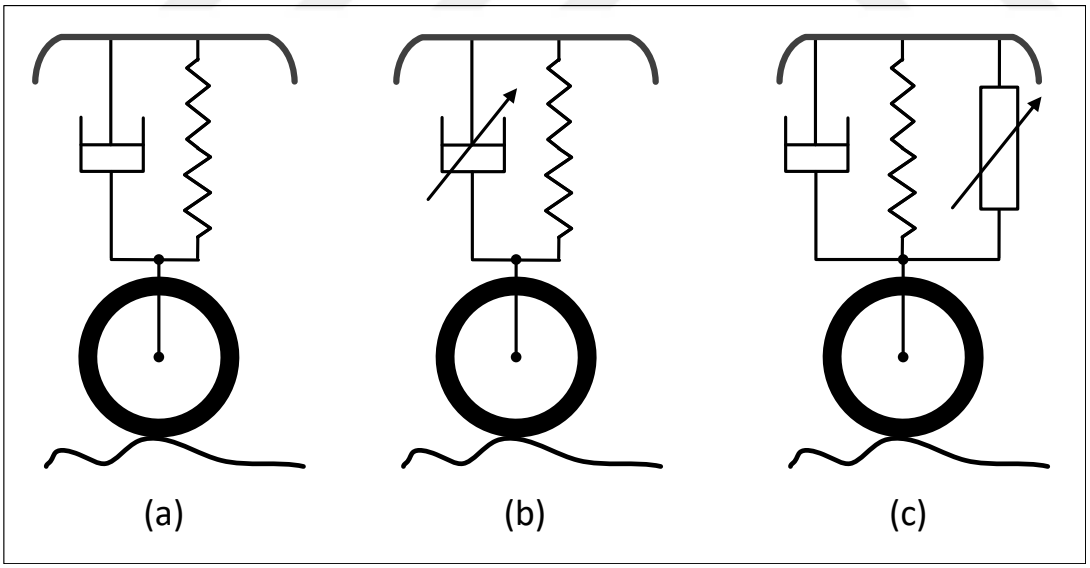

Figure 2.1: Suspension system types

2.3.2 Semi-Active

Semi-active suspension is a modified version of passive suspension (figure 2.1 part (b)). In this type, damping coefficient of the suspension is adjustable. Therefore, semi-active suspension can make the suspension stiffer or softer depending on the driving mode.

2.3.3 Active

Active suspension systems have a separate actuator (figure 2.1 part (c)), that can add or subtract force to the suspension system, independent of the passive components. In that sense, they are superior to semi-active ones. By improvements in actuator technology, it was possible for designers to design high quality hydraulic [5], hydro-pneumatic [6] and electromagnetic type active suspensions [7].

2.4 Active Suspension Background

The main objective of active suspension is to keep a balance between lowering sprung mass acceleration (better ride comfort), and suspension deflection (better handling).

2.4.1 Slow Active Suspension

Some active suspensions have low bandwidth around 5 Hz and below. The actuator in this kind is either hydraulic or electromagnetic in parallel with spring and damper. One example of slow active suspension is Mercedes Active Body Control (ABC) system. This system is hydraulic and it can reduce low-frequency roll and pitch movement and, can level vehicle up to 65 mm [8]. Zf and Volkswagen developed a slow active suspension with an electromagnetic actuator. Since the electromagnetic actuator can work as a generator also and regenerate waste energy, it has 4 times less energy consumption compared to the ABC system of Mercedes [9]. There is another kind of slow active suspension called low-power variable geometry active suspension system [10, 11]. In this system the vehicle body and tire are connected using a spring and a

wishbone. By using a permanent magnet DC motor, wishbone is rotated, changing the initial tension of spring. The change generates a variable active force in parallel with the spring. This system uses lower energy compared to the conventional active suspension.

2.4.2 Fast Active Suspension

Another kind of active suspension is fast active suspension. These systems have bandwidth of 50 Hz and more. The actuator is connected directly between sprung and unsprung mass. Sometimes a spring is placed in parallel with the actuator to handle vehicle weight and reduce energy consumption. Since the actuator exerts force directly to sprung and unsprung masses, it can achieve higher bandwidth considering that actuator has high bandwidth itself [8]. First fast active suspension was developed for Lotus Esprit which was later used for Lotus T92 Formula 1 car in 1983 [12]. This system had a hydraulic actuator and improved the Formula 1 car performance significantly. After this development in Lotus cars, active suspensions have attracted significant attention [13]. Another fast active electromagnetic suspension system is developed by a speaker company, Bose [14]. Their system had a linear actuator in parallel with a spring. It has a high bandwidth. It will be commercialized by ClearMotin MIT based company in 2020 [15].

2.5 Active Suspension Controller Design

Designing a decent controller for an active suspension system is as important as its mechanical design. It is a difficult task due to complicated relationships between suspension parts. Proper mathematical modeling of the suspension is crucial for designing a controller. In reality, there are non-linearities in the suspension system. Spring force has a non-linear relationship with suspension deflection [16], but up to a certain amount of deflection, it has linear behavior.

This behavior is shown in figure 2.2 for the springs used in this study. Suspension deflection is considered up to $0.25\ (m)$ in case of a SUV vehicle. So, for small deflections (smaller than $0.1\ (m)$) spring force can be considered to have linear relationship

with suspension deflection. But, for suspension deflection more than $0.1\ (m)$, the difference between linear consideration and non-linear consideration is large. This difference is shown in figure 2.3. The non-linear part of the spring force can go up to $500\ (N)$. This amount can happen for very rough roads or big bumps and holes.

Also, damper coefficient changes during bound and rebound and has discontinuous behavior [17]. This non-linearity is significant and has high effect on suspension dynamic behavior.

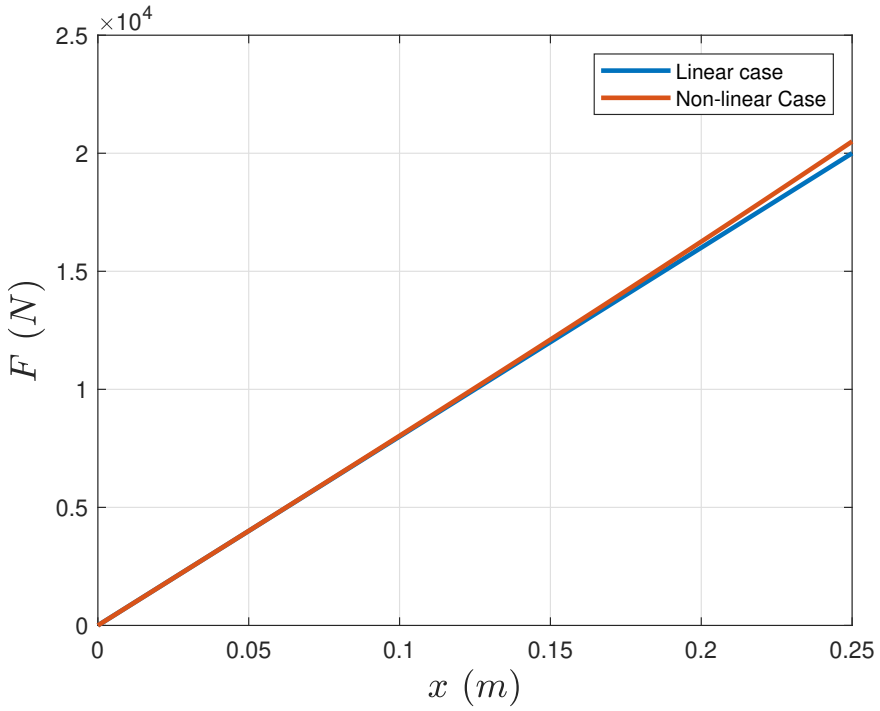

Figure 2.2: Non-linear and linear spring force vs deflection

There are other sources of non-linearity in suspension system. Damping coefficient may change due to suspension speed rather than its sign. Also, the friction in the damper is non-linear. Tire itself has some non-linearities. Tire stiffness can be non-linear. All mentioned non-linearities above are neglected in this study due to their small effect on dynamic behavior of the system.

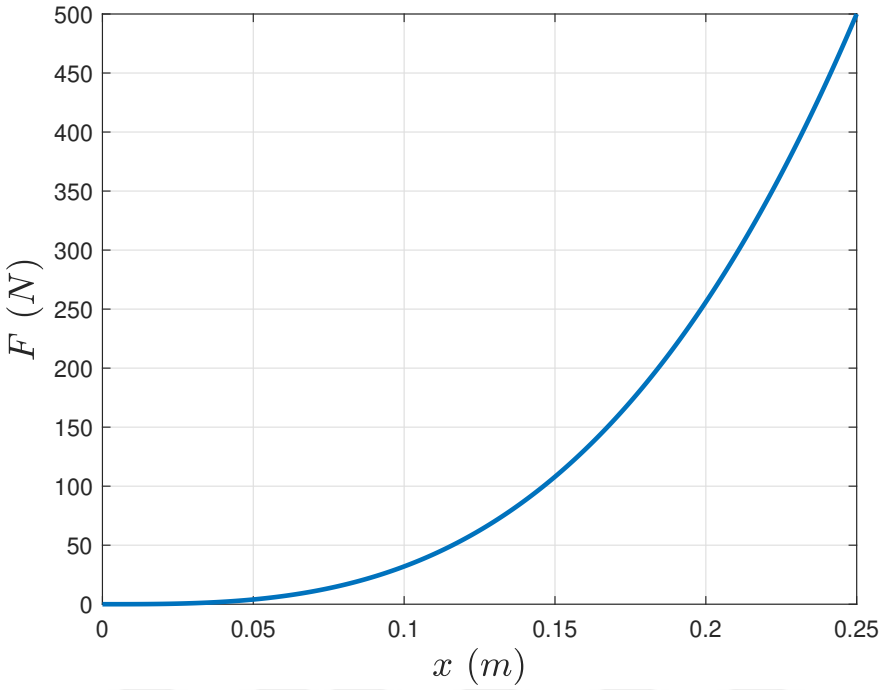

Figure 2.3: The non-linear part of the spring force vs deflection

2.5.1 Controller Design for Linear Systems

Many researchers neglect non-linearities of the suspension system for obtaining the mathematical model in order to avoid complicated mathematics of non-linear systems. By doing this accuracy of model decreases [18], but design procedure becomes easier [19]. Many controllers have been designed for linear systems in order to improve ride comfort and handling.

Hrovat did research on optimal control of active suspension systems [20]. Applications of optimal control techniques for design of active suspensions systems was investigated in this study. The control method applied is Linear–Quadratic optimal control.

Schwarzgruber et al. [21] designed a backstepping controller for an active suspension with a special class of Lyapunov functions. The method used is easily tunable for ride comfort and safety. Tuning the controller between ride comfort and handling is largely dependant on ω_g which is the low pass cut-off frequency of control Lyapunov

function. The proposed controller shows improved ride comfort for different road profiles.

Gysen et al. [22] investigated effect of using a direct-drive electromagnetic actuator on active suspension. A Linear Quadratic Regulator controller (LQR) was developed in this study. The designed controller under different road conditions provides significant improvement in ride comfort and handling.

Guo et al. [23] designed a robust H_∞ controller and used linear matrix inequality (LMI) optimization technique for an active suspension considering the standard colored noise road profile. A two DOF quarter car model with parameter uncertainty was used in this study. By using the theory of robust H_∞ controller, design procedure was converted into a constrained optimization problem, solved by using a group of LMIs. The proposed controller provides stability against non-stationary random road profile and parameter uncertainty, and improves ride comfort significantly.

Wang et al. [24] designed a fault-tolerant output-feedback H_∞ controller for a full car model subject to finite-frequency constraints of $4 - 8$ Hz. Actuator faults were also considered in this study. The designed controller could show improvement in both ride comfort and handling under constraints and different actuator faults.

Savaş et al. [5] designed adaptive control for hydraulic actuator using backstepping technique for an active suspension with unknown vehicle mass, tire stiffness and tire damping coefficient. Despite unknown system parameters and disturbance, the proposed controller drove the sprung mass acceleration to zero and improved ride comfort compared to the passive system.

Li et al. [25] studied an adaptive event-triggered T-S fuzzy control for an active suspension system considering uncertainties. Controller was designed considering actuator failure. Lyapunov theory was used to guarantee improvement in ride comfort. The proposed controller could improve ride comfort and lower suspension deflection significantly compared to passive suspension.

2.5.2 Controller Design for Non-linear Systems

As mentioned in section 2.5, actual force characteristic of spring and damper are non-linear, so although assuming them linear simplifies the system, accuracy gets sacrificed. Therefore non-linear model is used in many studies in literature, mentioned below.

Deshpande et al. [26] designed a new method in combination with sliding mode control to attenuate sprung mass acceleration. This method estimates the effect of all non-linearities, uncertainties and road profile with a good accuracy. The simulations and experiments for three different road profile and load variation showed that the sliding mode controller combined with disturbance observer, improves ride comfort while keeping road holding safety measures.

Pan et al. [27] designed a terminal sliding mode control for active suspension with hard constraints on suspension deflection and tire deflection. They overcome chattering and singularity issue of terminal sliding mode control by using chattering free second order reaching law. The proposed controller improved ride comfort significantly and showed better performance compared to conventional proportional differential (PD) controller.

Huang et al. [28] designed two adaptive controllers for an active suspension system with unknown non-linear dynamics (e.g., non-linear spring and piece-wise linear damper dynamics) and uncertain sprung mass. An augmented neural network is developed to compensate for the unknown non-linearities, and a novel adaptive law is developed to estimate both Neural Network weights and uncertain sprung mass. The second proposed controller which takes error convergence rate, maximum overshoot and steady-state error into account, acts slightly better and faster in attenuating sprung mass displacement compared to the first adaptive controller.

Sofiane et al. [29] proposed a novel robust non-linear multi-variable predictive controller developed for a non-linear quarter car model. The non-linear system is approximated by a linear one using the T-S fuzzy approach. Using LMIs the controller design is converted to constrained optimization problem. The proposed robust non-linear predictive control shows better performance in improving ride comfort com-

pared to model predictive control.

Rath et al. [30] designed an output feedback terminal sliding mode control considering a non-linear model of a hydraulic type active suspension. The proposed controller showed robustness under uncertainties and road disturbance and improved ride comfort without deteriorating handling.

Wen et al. [31] designed a sliding mode controller for an active suspension considering parameter uncertainty. The uncertain system was transformed to a summation of linear systems using T-S fuzzy method. The sliding surface and control law was developed based on this fuzzy system. The proposed controller shows improvement in ride comfort compared to passive system.

Wang et al. [32] designed a model predictive sliding mode controller for a non-linear active suspension. An output feedback sliding surface is designed. Non-linear terms are approximated by fuzzy logic. By using optimal and model predictive control theory, an adaptive sliding mode control law was designed to eliminate approximation errors. The proposed predictive sliding mode controller based on these approximations works with moderate accuracy and improves performance against uncertainties of the controller. The proposed controller shows improvement in ride comfort considering both sprung mass acceleration and pitch.

Pang et al. [33] designed a novel adaptive backstepping controller for a non-linear quarter car model which includes input delay and uncertain sprung mass. An adaptive control law that satisfies safety criteria of road holding is developed. The proposed controller can improve ride comfort significantly compared to conventional adaptive backstepping control and passive suspension in the presence of input delay.

Mrazgua et al. [34] designed a fuzzy fault-tolerant H_∞ control for a quarter car model considering actuator faults and parameter uncertainty. The uncertainty of the system is approximated and linearized using T-S fuzzy approach. Actuator faults are addressed using LMIs in designing the controller. The designed controller satisfies Lyapunov stability theory and constraints of the system alongside improving ride comfort with or without actuator failure.

Lin et al. [35] designed a fault tolerant controller for a non-linear quarter car model.

The system contains non-linearities, uncertainties, actuator and sensor faults, all with known boundaries. The original states are transformed to augmented states for simplicity of calculations. Then a new sliding mode observer is designed for the augmented state space. Finally a fault tolerant controller is designed for the system which improves ride comfort in the presence of actuator fault.

2.5.2.1 Optimal Sliding Mode Control

Sliding mode control is applied frequently for active suspension control in literature [26, 27, 31, 32]. But there is a special version of sliding mode control, named as "optimal sliding mode control" [36] which is very suitable for active suspension control purpose. The reason of this is that the Eigenvalues of the desired sliding mode motion is specified with respect to a cost function.

Zhang et al. [37] proposed a feedforward and feedback optimal sliding mode control for an active suspension considering random road profile. Using a cost function with weightings of suspension deflection, tire deflection and sprung mass velocity, an optimal sliding surface is designed. Based on non-linear reaching law, the equivalent control law is proposed. The proposed feedforward feedback optimal sliding mode control shows better performance in improving ride comfort, road holding and robustness compared to feedback optimal sliding mode control.

Later Chen et al. in 2017 [17] proposed an improved optimal siding mode control for a non-linear active suspension. Using feedback feedforward linearization method the system is linearized. By augmenting the sprung mass acceleration on top of the original states, an optimal sliding surface is designed. Based on a linear reaching law, the equivalent control law is proposed. The proposed controller shows improvement regarding ride comfort and robustness against different values of sprung mass and tire stiffness.

Zhou et al. [38] designed an optimal sliding mode control for a linear active suspension. They used genetic algorithm to find optimal weighting factors for suspension deflection, tire deflection and sprung mass acceleration. Using these optimal weighting factors optimal sliding surface is designed. The proposed controller improves ride

comfort more, compared to simple sliding mode control.

Both this work and previous work take sprung mass acceleration as one of the optimization criteria, although the Zhou method [38] does not explain clearly how the sprung mass acceleration is taken into the cost function for the OSMC, without taking it as a separate state. Following [37] work, in this study, optimization is done for tire deflection, suspension deflection and sprung mass velocity. In this sense there is no need to do the augmentation as in [17].

2.5.2.2 Considering System Uncertainties

In recent years compensating uncertainties in the suspension system, has gained attention. One of the most significant uncertainty in suspension system is sprung mass due to the change in number of the passengers and cargo. Some researchers have developed estimators for estimating these uncertainties, especially sprung mass.

In [26], sprung mass is divided into a nominal and a multiplicative uncertainty value. During designing the sliding manifold, this uncertainty is represented by an error variable and an observer is designed to estimate this error.

In [28] a novel adaptive law is developed to update the unknown sprung mass online, where the parameter estimation error is obtained. Also, [5] used the same technique by designing an adaptive controller and update laws for estimation of unknown parameters, sprung mass and tire stiffness.

Wen et al. [31], Li et al. [25] and Mrazgua et al. [34] addressed uncertainty in the system by utilizing T-S fuzzy model. Based on upper and lower limits of sprung mass, variable sprung mass is rewritten as a function of its upper and lower limits. Then membership functions are calculated and complex uncertain systems are viewed as the summation of a set of linear subsystems, which are solved by linear system theory.

Non-linear estimators are used more recently due to their performance against non-linear nature of suspension system. Pang et al. addressed uncertainty of sprung mass in some of their work. A new parameter is designed based on uncertain sprung mass and bounds are defined for it. This parameter is included in optimizing robust H_∞

controller in [39]. In [33, 40, 41] based on the non-linear active suspension model, an adaptive control law is developed to estimate the uncertain sprung mass online.

Some studies consider all possible uncertainties in the system as a lumped variable and design an estimator for it. In [35] a sliding mode observer was designed for estimating system uncertainties.

Gang [42] and Du [43] used an improved non-linear extended state observer with switching terms to estimate uncertainties.

Extended Kalman filter is a powerful non-linear state estimator which is used for parameter estimation as well. This estimator linearizes the non-linear system and computes the optimal state update gain. Only Koch et al. in [44] compared the performance of new estimation method [45] with an extended Kalman filter and simple filter based estimator. The proposed three parallel Kalman filter structure is better for estimating system states compared to extended Kalman filter. Yet extended Kalman filter still achieves an accurate estimate of the sprung mass. The previous comparison was done for passive system. This study uses extended Kalman filter for an active system. Also, in literature, effect of using nominal or incorrect sprung mass, in designing the controller, especially the optimal sliding mode control method, has not been investigated. This is the expected contribution of this work to literature.

CHAPTER 3

NON-LINEAR QUARTER CAR MODEL

3.1 Introduction

For vibration analysis of the vehicle, a mathematical model is needed. This mathematical model is obtained from the free body diagram of the vehicle and all the forces acting on the suspension and the vehicle. Since the vehicle is a complicated mechanical system, free body diagram of it contains many DOF. Choosing the simplest and the most proper model is necessary.

Quarter car model is the fundamental model used in designing suspension controllers. It is commonly used in semi-active and active suspension controller development studies [46]. This model addresses only one corner of the vehicle due to symmetric behavior of vehicle response during straight line driving. Therefore, it is limited to body bounce motion only. It is not capable of representing pitch and roll motion.

3.2 Quarter Car Model of the Passive Suspension

Quarter car model is illustrated in figure 3.1. This model is a 2 DOF model, consisting of unsprung mass and a quarter of the sprung mass.

3.2.1 Parameters

Parameters of the model are these:

- m_u is the unsprung mass and it is the mass of the Wheel assembly and part of

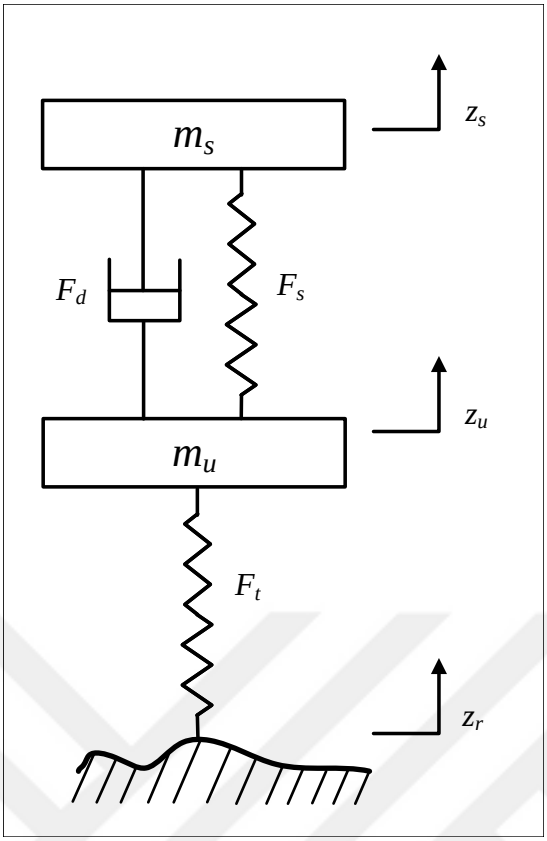

Figure 3.1: Quarter car model of a passive suspension

the suspension itself.

- m_s is the sprung mass and its value is one quarter of the vehicle sprung mass.
- z_s is the DOF associated with the vertical motion of the sprung mass.
- z_u is the DOF associated with the vertical motion of the unsprung mass.
- z_r is the vertical displacement of the tire due to the road profile.
- F_s is the suspension spring force.
- F_d is the suspension damper force.
- F_t is the tire force.

The quarter car model used in this study is non-linear [17]. The non-linear terms are the spring force and the damper force.

3.2.2 Spring Force

Spring force is:

$$F_S(d_{s0} + z_s - z_u) = k_{1s}(d_{s0} + z_s - z_u) + k_{2s}(d_{s0} + z_s - z_u)^3 \tag{3.1}$$

Where k_{1s} and k_{2s} are the linear and non-linear spring stiffness coefficients respectively. Also, d_{s0} is the static suspension deflection.

3.2.3 Damper Force

Also the suspension damper force exhibits a non-linear force characteristic. Damper force is:

$$F_d(\dot{z_s} - \dot{z_u}) = \begin{cases} c_{1s}(\dot{z_s} - \dot{z_u})\ if\ \dot{z_s} - \dot{z_u} \geq 0 \\ c_{2s}(\dot{z_s} - \dot{z_u})\ if\ \dot{z_s} - \dot{z_u} < 0 \end{cases} \tag{3.2}$$

Where c_{1s} and c_{2s} are the damping coefficients of the damper during expansion and compression respectively. Damping coefficient is typically higher during rebound phase compared to bump phase [47]. This asymmetric behavior is expressed with equation 3.2. This expression is replaced by a continuous function as follows:

$$c_s = \Delta c_s \operatorname{sgn}(\dot{z_s} - \dot{z_u}) + \bar{c}_s \tag{3.3}$$

where

$$\Delta c_s = \frac{c_{1s} - c_{2s}}{2} \tag{3.4}$$

$$\bar{c}_s = \frac{c_{1s} + c_{2s}}{2} \tag{3.5}$$

Arctangent function is used here to approximate the sign function with a differentiable one. This is especially important for controller development purposes, such as checking the rank of the controllability & observability matrices, as explained in [48].

$$c_s = \Delta c_s \tan^{-1}\left(1000(\dot{z_s} - \dot{z_u})\right) + \bar{c}_s \tag{3.6}$$

The argument inside the arctangent function has a high multiplier value to make it more similar to the sign function. Damping coefficient given in equation 3.6, using values presented in table 6.2, is given in figure 3.2.

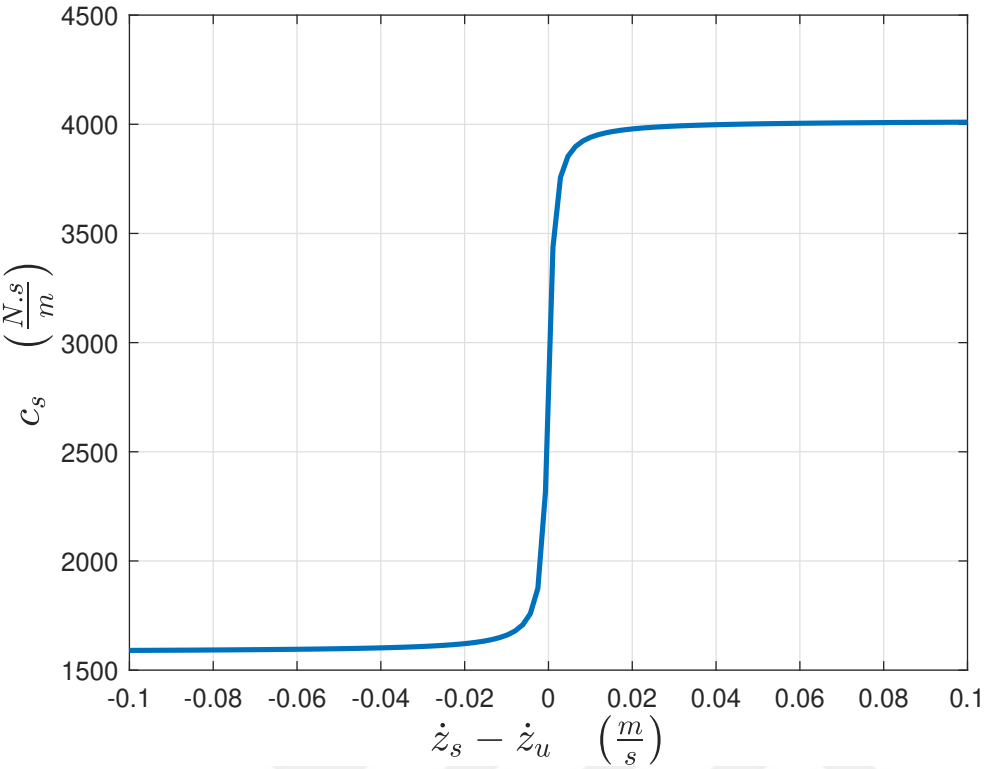

Figure 3.2: Typical asymmetrical damper force characteristic

3.2.4 Tire Force

Tire force is:

$$F_t = k_t(d_{t0} + z_u - z_r) \tag{3.7}$$

Where k_t is the tire stiffness coefficient and d_{t0} is the tire static deflection.

3.2.5 Equations of Motion

Equations of motion are written with respect to origin of the motion coordinates since the system is non-linear. Static deflections can be obtained by:

$$m_s g + F_s(d_{s0}) = 0 \tag{3.8}$$

$$(m_s + m_u)g + k_t d_{t0} = 0 \tag{3.9}$$

Equations of motion for the dynamic behavior of the non-linear quarter car model are expressed as:

$$m_s\ddot{z_s} = -F_s - F_d - m_s g \tag{3.10}$$

$$m_u\ddot{z_u} = F_s + F_d - F_t - m_u g \tag{3.11}$$

which are second order ordinary differential equations. By substituting equations 3.1 to 3.9 into equations of motion, the following equations can be obtained.

Equation of motion for the sprung mass is:

$$\begin{aligned} m_s\ddot{z_s} + k_{1s}(d_{s0} + z_s - z_u) + k_{2s}(d_{s0} + z_s - z_u)^3 \\ -k_{1s}d_{s0} - k_{2s}d_{s0}^3 + c_s(\dot{z_s} - \dot{z_u}) = 0 \end{aligned} \tag{3.12}$$

And the equation of motion for the unsprung mass is:

$$\begin{aligned} m_u\ddot{z_u} - k_{1s}(d_{s0} + z_s - z_u) - k_{2s}(d_{s0} + z_s - z_u)^3 + k_{1s}d_{s0} + k_{2s}d_{s0}^3 \\ -c_s(\dot{z_s} - \dot{z_u}) + k_t(z_u - z_r) = 0 \end{aligned} \tag{3.13}$$

3.2.6 State Space Representation

In order to investigate the behavior of the suspension, equations of motion obtained in previous section (equations 3.12 and 3.13) should be presented in the state space form. For this, proper state variable selection is vital.

State variables are chosen with the objective of representing the most important variables regarding vehicle suspension. First state variable is tire deflection, second one is suspension deflection and the third and forth ones are unsprung and sprung mass speeds. Therefore state vector is:

$$\mathbf{x} = \begin{bmatrix} x_1 & x_2 & x_3 & x_4 \end{bmatrix}^T \tag{3.14}$$

where state variables are:

$$\begin{aligned} x_1 &= z_r - z_u \\ x_2 &= z_u - z_s \\ x_3 &= \dot{z_u} \\ x_4 &= \dot{z_s} \end{aligned} \tag{3.15}$$

State space equations for non-linear systems in the presence of the disturbance and measurement noise can be expressed as:

$$\dot{\mathbf{x}} = \mathbf{f}(\mathbf{x}, \omega) \tag{3.16a}$$

$$\mathbf{y} = \mathbf{h}(\mathbf{x}) + \mathbf{v} \tag{3.16b}$$

Where ω is disturbance. Outputs of the system are sprung mass acceleration $(\ddot{z_S})$ and unsprung mass acceleration $(\ddot{z_u})$ and **v** is measurement noise vector. By using state variables defined in equation 3.15 and substituting those in equations 3.12 and 3.13, non-linear state space representation in the form of equation 3.16 can be obtained:

$$\begin{Bmatrix} \dot{x_1} \\ \dot{x_2} \\ \dot{x_3} \\ \dot{x_4} \end{Bmatrix} = \begin{Bmatrix} -x_3 \\ x_3 - x4 \\ \frac{k_t x_1 + k_{1s}(d_{s0} - x_2) + k_{2s}(d_{s0} - x_2)^3 + m_s g + c_s(x_4 - x_3)}{m_u} \\ \frac{-k_{1s}(d_{s0} - x_2) - k_{2s}(d_{s0} - x_2)^3 - m_s g - c_s(x_4 - x_3)}{m_s} \end{Bmatrix} + \begin{Bmatrix} 1 \\ 0 \\ 0 \\ 0 \end{Bmatrix} \dot{z_r} \tag{3.17}$$

And the outputs are:

$$\begin{Bmatrix} y_1 \\ y_2 \end{Bmatrix} = \begin{Bmatrix} \frac{k_t x_1 + k_{1s}(d_{s0} - x_2) + k_{2s}(d_{s0} - x_2)^3 + m_s g + c_s(x_4 - x_3)}{m_u} \\ \frac{-k_{1s}(d_{s0} - x_2) - k_{2s}(d_{s0} - x_2)^3 - m_s g - c_s(x_4 - x_3)}{m_s} \end{Bmatrix} + \begin{Bmatrix} v_1 \\ v_2 \end{Bmatrix} \tag{3.18}$$

where

$$c_s = \Delta c_s \tan^{-1}\left(1000(x_4 - x_3)\right) + \bar{c}_s \tag{3.19}$$

and v_1 and v_2 represent zero mean white noise, associated with the acceleration measurements, with covariances R_1 and R_2, respectively. The time derivative of the road profile, $\dot{z_r}$, on the other hand, is treated as the disturbance and has a process noise with the covariance of Q, which is used in designing the extended Kalman filter in the next chapter. So, the non-linear state space representation of equation 3.16, for the system of this study is rearranged as:

$$\dot{\mathbf{x}} = \mathbf{f}(\mathbf{x}) + \mathbf{G}\boldsymbol{\omega} \tag{3.20}$$

$$\mathbf{y} = \mathbf{h}(\mathbf{x}) + \mathbf{v} \tag{3.21}$$

where $\mathbf{f}_{4\times1}$ is state vector, $\mathbf{G}_{4\times1}$ is disturbance input matrix and ω is the disturbance. $\mathbf{h}_{2\times1}$ is output measurement vector and $\mathbf{v}_{2\times1}$ is measurement noise vector. Each term

is described in detail as follows:

$$\mathbf{f} = \begin{Bmatrix} -x_3 \\ x_3 - x4 \\ \frac{k_t x_1 + k_{1s}(d_{s0} - x_2) + k_{2s}(d_{s0} - x_2)^3 + m_s g + c_s(x_4 - x_3)}{m_u} \\ \frac{-k_{1s}(d_{s0} - x_2) - k_{2s}(d_{s0} - x_2)^3 - m_s g - c_s(x_4 - x_3)}{m_s} \end{Bmatrix} \tag{3.22}$$

$$\mathbf{G} = \begin{bmatrix} 1 & 0 & 0 & 0 \end{bmatrix}^T \tag{3.23}$$

$$\omega = z_r \tag{3.24}$$

$$\mathbf{h} = \begin{Bmatrix} \frac{k_t x_1 + k_{1s}(d_{s0} - x_2) + k_{2s}(d_{s0} - x_2)^3 + m_s g + c_s(x_4 - x_3)}{m_u} \\ \frac{-k_{1s}(d_{s0} - x_2) - k_{2s}(d_{s0} - x_2)^3 - m_s g - c_s(x_4 - x_3)}{m_s} \end{Bmatrix} \tag{3.25}$$

$$\mathbf{V} = \begin{bmatrix} v_1 & v_2 \end{bmatrix}^T \tag{3.26}$$

3.3 Quarter Car Model of the Active Suspension

The quarter car model of the active suspension is same as the passive suspension, with the addition of an actuator, shown in figure 3.3. This actuator is capable of exerting force in both directions. Since every part of the system is same as the passive one, all forces on the system can be obtained from the equations presented in the previous section.

3.3.1 Actuator Force

The actuator force, F_a, is first calculated by the controller unit of the active suspension (which will be discussed later) and then exerted to the system by the actuator. Using this extra force, system becomes active and acts in the same or opposite direction to the suspension forces, and achieves the desired ride comfort level.

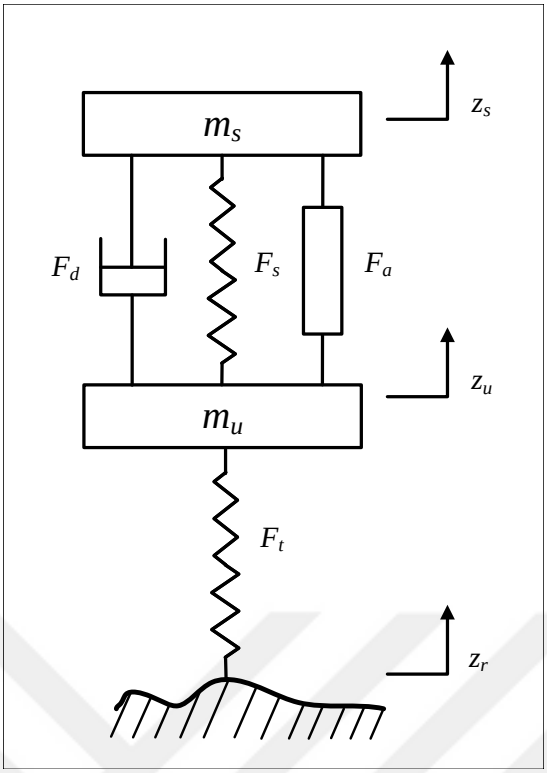

Figure 3.3: Quarter car model of an active suspension

3.3.2 Equations of Motion

Equations of motions are same as passive system except that now F_a is present.

$$m_s\ddot{z}_s = -F_s - F_d - m_s g + F_a \tag{3.27}$$

$$m_u\ddot{z}_u = F_s + F_d - F_t - m_u g - F_a \tag{3.28}$$

F_a default acting mode has been chosen such that it pushes sprung mass upward (shown with a positive sign in equation 3.27) and unsprung mass downward (shown with a negative sign in equation 3.28). Based on equations 3.6, 3.12 and 3.13, equations of motion for the active suspension are obtained. Equation of motion for the sprung mass is:

$$\begin{aligned} m_s\ddot{z}_s + k_{1s}(d_{s0} + z_s - z_u) + k_{2s}(d_{s0} + z_s - z_u)^3 \\ -k_{1s}d_{s0} - k_{2s}d_{s0}^3 + c_s(\dot{z}_s - \dot{z}_u) = F_a \end{aligned} \tag{3.29}$$

And the equation of motion for the unsprung mass is:

$$\begin{aligned} m_u\ddot{z}_u - k_{1s}(d_{s0} + z_s - z_u) - k_{2s}(d_{s0} + z_s - z_u)^3 + k_{1s}d_{s0} + k_{2s}d_{s0}^3 \\ -c_s(\dot{z}_s - \dot{z}_u) + k_t(z_u - z_r) = -F_a \end{aligned} \tag{3.30}$$

3.3.3 State Space Representation

In order to to design a controller, equations of motion obtained in previous section (equations 3.29 and 3.30) should be presented in the state space form, again. For this, state variables defined for passive suspension (equation 3.15) are applicable. State space equations for non-linear systems based on equation 3.16 for controller system is:

$$\dot{\mathbf{x}} = \mathbf{f}(\mathbf{x}, u, \omega) \tag{3.31a}$$

$$\mathbf{y} = \mathbf{h}(\mathbf{x}, u) + \mathbf{v} \tag{3.31b}$$

where u is the control input and ω is the disturbance. Outputs of the system are sprung mass acceleration $(\ddot{z_S})$ and unsprung mass acceleration $(\ddot{z_u})$ and $\mathbf{v}$ is measurement noise vector again. By using state variables defined in equation 3.15 and substituting those in equations 3.29 and 3.30, non-linear state space representation in the form of equation 3.31 can be obtained:

$$\begin{Bmatrix} \dot{x_1} \\ \dot{x_2} \\ \dot{x_3} \\ \dot{x_4} \end{Bmatrix} = \begin{Bmatrix} -x_3 \\ x_3 - x4 \\ \frac{k_t x_1 + k_{1s}(d_{s0} - x_2) + k_{2s}(d_{s0} - x_2)^3 + m_s g + c_s(x_4 - x_3)}{m_u} \\ \frac{-k_{1s}(d_{s0} - x_2) - k_{2s}(d_{s0} - x_2)^3 - m_s g - c_s(x_4 - x_3)}{m_s} \end{Bmatrix} + \begin{Bmatrix} 0 \\ 0 \\ \frac{-1}{m_u} \\ \frac{1}{m_s} \end{Bmatrix} F_a + \begin{Bmatrix} 1 \\ 0 \\ 0 \\ 0 \end{Bmatrix} \dot{z_r} \tag{3.32}$$

And the output equations are:

$$\begin{Bmatrix} y_1 \\ y_2 \end{Bmatrix} = \begin{Bmatrix} \frac{k_t x_1 + k_{1s}(d_{s0} - x_2) + k_{2s}(d_{s0} - x_2)^3 + m_s g + c_s(x_4 - x_3)}{m_u} \\ \frac{-k_{1s}(d_{s0} - x_2) - k_{2s}(d_{s0} - x_2)^3 - m_s g - c_s(x_4 - x_3)}{m_s} \end{Bmatrix} + \begin{Bmatrix} \frac{-1}{m_u} \\ \frac{1}{m_s} \end{Bmatrix} F_a + \begin{Bmatrix} v_1 \\ v_2 \end{Bmatrix} \tag{3.33}$$

where c_s (equation 3.19), v_1, v_2 and $\dot{z_r}$ are described in section 3.2.6. So, the non-linear state space representation of equation 3.31 for the active system can be arranged as:

$$\dot{\mathbf{x}} = \mathbf{f}(\mathbf{x}) + \mathbf{B}u + \mathbf{G}\boldsymbol{\omega} \tag{3.34}$$

$$\mathbf{y} = \mathbf{h}(\mathbf{x}) + \mathbf{D}u + \mathbf{v} \tag{3.35}$$

Where **f**, **G**, $\boldsymbol{\omega}$, **h** and **v** are same as equations 3.22 to 3.26. Only new matrices are $\mathbf{B}_{4\times1}$, which is the control input matrix and $\mathbf{D}_{2\times1}$, which is feedforward matrix. These

matrices are given below.

$$\mathbf{B} = \begin{bmatrix} 0 & 0 & \frac{-1}{m_u} & \frac{1}{m_s} \end{bmatrix}^T \tag{3.36}$$

$$\mathbf{D} = \begin{bmatrix} \frac{-1}{m_u} & \frac{1}{m_s} \end{bmatrix}^T \tag{3.37}$$

CHAPTER 4

SPRUNG MASS ESTIMATION

4.1 Introduction

As described in chapter 1, one of the uncertainties of the system, is the sprung mass. The unloaded mass of the vehicle may increase due to the weight of passengers and cargo. Considering the vehicle that is takes into account in this thesis, the cargo weight may go up to $2000kg$. So, sprung mass would change drastically and effect the dynamics of the system.

The design procedure can be applied considering an unloaded (with only the driver in it), half-loaded or a full-loaded vehicle. However, these approaches do not represent the sprung mass correctly considering all drive cycles of the vehicle. The ideal case is designing the controller for the correct sprung mass and the proof for this statement will be presented in chapter 7.

4.2 Effects of Incorrect Information for Sprung Mass

First effect of the sprung mass change is on the state estimator (section 5.8). Estimator uses vehicle parameters and measurements to estimate state variables. Having one of the most important vehicle parameters incorrect in the estimation algorithm, would cause incorrect estimations result. This in turn, would effect the controller performance.

Second effect is on the coefficients of the optimal sliding surface (section 5.5). Sliding surface coefficients, i.e. eigenvalues of the closed loop system strictly depends on the

sprung mass value. So, any incorrect information of the sprung mass would cause the controller to act out of its predefined criteria. This effect will be discussed in chapter 7.

Third effect is on the de-linearization stage. In this stage, linearized control input v_2, is transformed back to the original non-linear control input F_a, given by the expression in equation 5.53. Sprung mass m_S, is used in this equation, so any incorrect sprung mass information would result in incorrect F_a and therefore deterioration of the control action.

Due to the reasons discussed, it is necessary to have a correct information of sprung mass. In this study, sprung mass is estimated using a parameter estimator. During parameter estimation, system is passive and obeys equation 3.16. Then the controller (which includes OSMC, state estimator and de-linearization blocks) is initiated using the correct information of sprung mass.

4.3 New State Space

The parameter estimator that is used in this study is "Extended Kalman Filter" due to its ability to coupe with non-linear systems [49]. In the estimator algorithm, sprung mass is treated as a separate state. On the other hand, since it is a function of static suspension deflection d_{s0} (equation 4.1 which is derived from equation 3.8), it is more appropriate to take d_{S0} as a separate state instead of m_s in the estimation algorithm.

$$m_S = \frac{-k_{1s}d_{s0} - k_{2s}d_{s0}^3}{g} \tag{4.1}$$

By choosing d_{s0} as the fifth state in addition to states described in equation 3.15, the new state variables can be written as:

$$\mathbf{x} = [x_1\ x_2\ x_3\ x_4\ x_5]^T \tag{4.2}$$

$$\begin{aligned} x_1 &= z_r - z_u \\ x_2 &= z_u - z_s \\ x_3 &= \dot{z_u} \\ x_4 &= \dot{z_s} \\ x_5 &= d_{s0} \end{aligned} \tag{4.3}$$

And the non-linear state equations 3.17 become:

$$\begin{Bmatrix} \dot{x_1} \\ \dot{x_2} \\ \dot{x_3} \\ \dot{x_4} \\ \dot{x_5} \end{Bmatrix} = \begin{Bmatrix} -x_3 \\ x_3 - x4 \\ \frac{k_t x_1 + k_{1s}(x_5 - x_2) + k_{2s}(x_5 - x_2)^3 - k_{1s}x_5 - k_{2s}x_5^3 + c_s(x_4 - x_3)}{m_u} \\ g\frac{-k_{1s}(x_5 - x_2) - k_{2s}(x_5 - x_2)^3 + k_{1s}x_5 + k_{2s}x_5^3 - c_S(x_4 - x_3)}{-k_{1s}x_5 - k_{2s}x_5^3} \\ 0 \end{Bmatrix} + \begin{bmatrix} 1 & 0 \\ 0 & 0 \\ 0 & 0 \\ 0 & 0 \\ 0 & 1 \end{bmatrix} \begin{Bmatrix} \dot{z_r} \\ w \end{Bmatrix} \tag{4.4}$$

where w is the process noise due to the uncertainty of d_{s0} variation. The new output equations are:

$$\begin{Bmatrix} y_1 \\ y_2 \end{Bmatrix} = \begin{Bmatrix} \frac{k_t x_1 + k_{1s}(x_5 - x_2) + k_{2s}(x_5 - x_2)^3 - k_{1s}x_5 - k_{2s}x_5^3 + c_s(x_4 - x_3)}{m_u} \\ g\frac{-k_{1s}(x_5 - x_2) - k_{2s}(x_5 - x_2)^3 + k_{1s}x_5 + k_{2s}x_5^3 - c_s(x_4 - x_3)}{-k_{1s}x_5 - k_{2s}x_5^3} \end{Bmatrix} + \begin{Bmatrix} v_1 \\ v_2 \end{Bmatrix} \tag{4.5}$$

4.4 Observability of the Non-linear System

Parameter estimator is an observer, and for designing any observer for a system, first observability of it should be checked. A non-linear system is said to be locally observable if the observability matrix **O** is full rank [48].

$$\mathbf{O} = \frac{\partial \mathbf{G}}{\partial \mathbf{x}} \tag{4.6}$$

where **G** is a set, consisting of all successive Lie derivatives of output function vector **h**, with respect to system vector **f**:

$$\mathbf{G} = \begin{bmatrix} L_f^0\mathbf{h} & L_f^1\mathbf{h} & L_f^2\mathbf{h} & L_f^3\mathbf{h} & L_f^4\mathbf{h} \end{bmatrix}^T \tag{4.7}$$

where:

$$L_f^0 h(\mathbf{x}) = h(\mathbf{x}) \tag{4.8a}$$

$$L_f h(\mathbf{x}) = \frac{\partial h(\mathbf{x})}{\partial \mathbf{x}} \mathbf{f}(\mathbf{x}) \tag{4.8b}$$

$$L_f^2 h(\mathbf{x}) = \frac{\partial L_f h(\mathbf{x})}{\partial \mathbf{x}} \mathbf{f}(\mathbf{x}) \tag{4.8c}$$

$$L_f^k h(\mathbf{x}) = \frac{\partial L_f^{k-1} h(\mathbf{x})}{\partial \mathbf{x}} \mathbf{f}(\mathbf{x}) \tag{4.8d}$$

$$L_f L_g h(\mathbf{x}) = \frac{\partial L_f h(\mathbf{x})}{\partial \mathbf{x}} \mathbf{g}(\mathbf{x}) \tag{4.8e}$$

The rank of the $\mathbf{O}$ matrix should be evaluated for all values of $\mathbf{x}$ for which the estimation algorithm is active. The rank of the $\mathbf{O}_{10\times5}$ matrix is calculated and plotted in figure 4.1 for the whole duration of simulation. As it is seen from the figure rank is always full, meaning the system is locally observable considering all operation points. Therefore it is possible to design a non-linear observer, or an extended Kalman filter for this system.

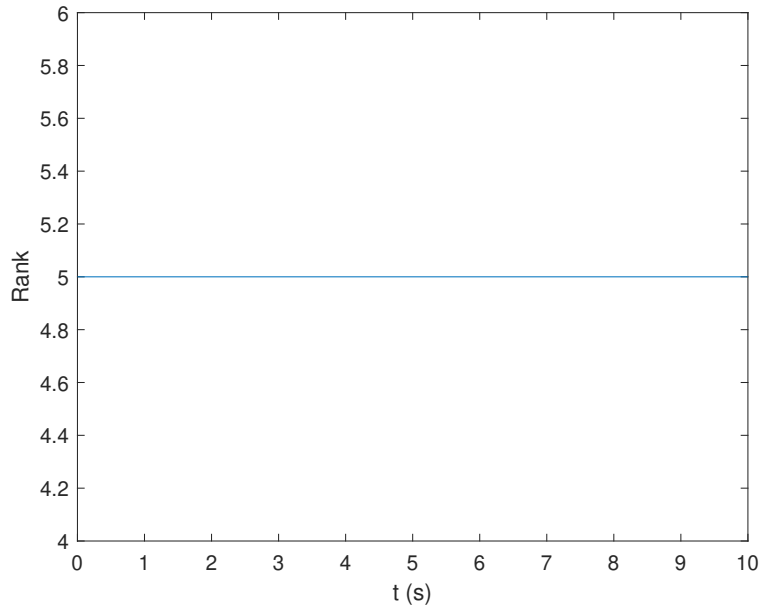

Figure 4.1: Rank of observability matrix $\mathbf{O}_{10\times5}$ for all time steps

4.5 Extended Kalman Filter

For estimating states from outputs, which are sprung and unsprung mass accelerations, as mentioned earlier, an extended Kalman filter is used. This estimator linearizes the non-linear system, and applies Kalman filter to it [50]. The state equation of 3.16 are discretized as:

$$\hat{\mathbf{x}}_{k+1} = \hat{\mathbf{x}}_k + \tau\, \dot{\hat{\mathbf{x}}}_k \tag{4.9}$$

where τ is time step of discretization and $\hat{\mathbf{x}}$ is estimated states vector. Notice that the only disturbance of the system is $\dot{z}_r$, so it will be multiplied by τ also. On the other hand w represents uncertainty associated with the variation of the fifth state, d_{s0}. Linearization is done by using Taylor series expansion, for non-linear terms of system in the form of equations 4.4, 4.5.

$$\mathbf{F}(\hat{\mathbf{x}}, k) = \frac{\partial \hat{\mathbf{x}}_{k+1}}{\partial \mathbf{x}}|_{\mathbf{x}=\hat{\mathbf{x}}_{k|k}} \tag{4.10}$$

$$\mathbf{H}(\hat{\mathbf{x}}, k) = \frac{\partial \mathbf{h}}{\partial \mathbf{x}}|_{\mathbf{x}=\hat{\mathbf{x}}_{k|k-1}} \tag{4.11}$$

W and **V** matrices are:

$$\mathbf{W} = \frac{\partial \hat{\mathbf{x}}_{k+1}}{\partial \omega} = \begin{bmatrix} \tau & 0 & 0 & 0 & 0 \\ 0 & 0 & 0 & 0 & \tau \end{bmatrix}^T \tag{4.12}$$

$$\mathbf{V} = \frac{\partial \mathbf{y}}{\partial v} = \begin{bmatrix} 1 & 0 \\ 0 & 1 \end{bmatrix} \tag{4.13}$$

Extended Kalman filter procedure is comprised of two steps, prediction and correction. It first predicts states and estimation error covariance **P** from knowledge of states and measurements up to the current step, and then corrects those with calculated Kalman gain **K** and measurements from current step.

Extended Kalman filter algorithm for discrete system is:

1. State prediction based on the previous estimated states:

$$\hat{\mathbf{x}}_{k|k-1} = \hat{\mathbf{x}}_{k-1|k-1} + \tau\, \mathbf{f}(\hat{\mathbf{x}}_{k-1|k-1}) \tag{4.14}$$

2. Prediction of estimation error covariance:

$$\mathbf{P}_{k|k-1} = \mathbf{F}_{k-1|k-1}\, \mathbf{P}_{k-1|k-1}\, \mathbf{F}^T_{k-1|k-1} + \mathbf{W}\, \mathbf{Q}\, \mathbf{W}^T \tag{4.15}$$

3. Computing Kalman gain:

$$\mathbf{K}_k = \mathbf{P}_{k|k-1}\,\mathbf{H}_{k|k-1}^T \Big[\mathbf{H}_{k|k-1}\,\mathbf{P}_{k|k-1}\,\mathbf{H}_{k|k-1}^T + \mathbf{V}\,\mathbf{R}\,\mathbf{V}^T\Big]^{-1} \tag{4.16}$$

4. Updating estimated states with measurements from current step:

$$\hat{\mathbf{x}}_{k|k} = \hat{\mathbf{x}}_{k|k-1} + \mathbf{K}_k\Big(\mathbf{y}_k - \mathbf{h}(\hat{\mathbf{x}}_{k|k-1})\Big) \tag{4.17}$$

5. Updating estimation error covariance:

$$\mathbf{P}_{k|k} = \mathbf{P}_{k|k-1} - \mathbf{K}_k\,\mathbf{H}_{k|k-1}\,\mathbf{P}_{k|k-1} \tag{4.18}$$

In equations above, $\mathbf{Q}_{2\times2}$ is process noise covariance matrix and $\mathbf{R}_{2\times2}$ is measurements noise covariance matrix. For the system of this study those are:

$$\mathbf{Q} = \begin{bmatrix} Q_1 & 0 \\ 0 & Q_5 \end{bmatrix} \tag{4.19}$$

$$\mathbf{R} = \begin{bmatrix} R_1 & 0 \\ 0 & R_2 \end{bmatrix} \tag{4.20}$$

where Q_1 is road profile velocity covariance, Q_5 is d_{s0} process noise covariance and R_1 and R_2 are unsprung mass accelerometer and sprung mass accelerometer noise covariances respectively.

CHAPTER 5

OPTIMAL SLIDING MODE CONTROLLER

5.1 Introduction to Sliding Mode Control

In dynamical systems with control law as a discontinuous function of states, a phenomena happens which is called "sliding mode". It happens in systems with high frequency switching control action [36].

Sliding mode control is a non-linear control technique having interesting properties such as accuracy, robustness, and easy tuning and implementation [51]. Sliding mode systems are designed to drive the system states onto a particular surface. This particular surface is called "sliding surface". Once the trajectory reaches the sliding surface, sliding mode control keeps the trajectory on a close neighbourhood of the sliding surface. Trajectory of states is kept in a certain distance from the sliding surface and keeps moving around it, that is why it is called "sliding mode".

Therefore the sliding mode controller design has two parts. The first part is to design a sliding surface so that the sliding motion satisfies design specifications. The second part is the selection of a control law that will make the trajectory move toward the sliding surface and keep around it [36].

There are two main advantages of sliding mode control. First one is that the dynamic behaviour of the system can be controlled by the particular choice of the sliding surface. Secondly, the closed loop system response becomes robust against particular uncertainties. These are parameter uncertainties, bounded disturbance and non-linearities. From a practical stand point sliding mode control allows controlling non-linear processes, subject to external disturbances and model uncertainties [51].

These features of sliding mode control makes it a suitable choice for the system of this study. The main disturbance is the road profile itself, uncertainty is sprung mass variation and the non-linearities are the spring and damper forces.

5.2 Optimal Sliding Mode Definition

The Concept of optimal sliding mode control is designing the sliding surface such that it minimizes a certain cost function. The sliding surface considered in this study, is chosen as a linear feedback of states:

$$S = \mathbf{C}\mathbf{x} \tag{5.1}$$

Where $\mathbf{C}_{1\times 4}$ is the sliding surface's coefficients matrix and S is the sliding surface. Sliding mode occurs on the sliding manifold where $S = 0$. Defining the coefficients of the sliding surface $\mathbf{C}$, is similar to defining the state feedback gain $\mathbf{K}$ (5.3), of a linear system of, give as equation 5.2.

$$\dot{\mathbf{x}} = \mathbf{A}\mathbf{x} + \mathbf{B}u \tag{5.2}$$

$$u = -\mathbf{K}\mathbf{x} \tag{5.3}$$

That is why $\mathbf{C}$ is chosen based on optimal control theory. The cost function subject to minimization is defined as:

$$J = \int_0^\infty [\mathbf{x}^T\mathbf{Q}\mathbf{x} + \mathbf{u}^T\mathbf{R}\mathbf{u}]dt \tag{5.4}$$

Where the first term represents the accuracy of the control action and the second term represents the control energy. $\mathbf{Q}_{n\times n}$ is a positive definite weighting matrix and $\mathbf{R}_{m\times m}$ is a positive definite, control effort weighting matrix. Normally optimal control gain which minimizes the J is obtained by linear quadratic regulator approach. But when the system involves non-linearities, J cannot be stated by equation 5.4 and be solved by classical linear quadratic regulator approach. So, it needs to be linearized [17]. That is why the non-linear system of this study (equation 3.34) is linearized. The procedure of linearization is discussed in the next section.

5.3 Feedback Linearization of the Non-linear System

The procedure described in [17] is applied using feedback linearization method originally described by [52] and explained in [53]. The non-linear system given by equation 3.32 is linearized as follows:

$$\dot{\mathbf{x}} = \mathbf{A}\mathbf{x} + \mathbf{B}u + \boldsymbol{\zeta}\dot{z}_r \tag{5.5}$$

$$\mathbf{y} = \mathbf{C}\mathbf{x} + \mathbf{D}u \tag{5.6}$$

where u is the linearizing control input containing all the non-linearities of the system in it:

$$u = \frac{-k_{1s}(d_{s0} - x_2) - k_{2s}(d_{s0} - x_2)^3 - m_s g - c_s(x_4 - x_3) + F_a}{m_s} \tag{5.7}$$

and

$$\mathbf{A} = \begin{bmatrix} 0 & 0 & -1 & 0 \\ 0 & 0 & 1 & -1 \\ \frac{k_T}{m_u} & 0 & 0 & 0 \\ 0 & 0 & 0 & 0 \end{bmatrix} \tag{5.8}$$

$$\mathbf{B} = \begin{bmatrix} 0 & 0 & -\frac{m_s}{m_u} & 1 \end{bmatrix}^T \tag{5.9}$$

$$\boldsymbol{\zeta} = \begin{bmatrix} 1 & 0 & 0 & 0 \end{bmatrix}^T \tag{5.10}$$

$$\mathbf{C} = \begin{bmatrix} \frac{k_T}{m_u} & 0 & 0 & 0 \\ 0 & 0 & 0 & 0 \end{bmatrix} \tag{5.11}$$

$$\mathbf{D} = \begin{bmatrix} -\frac{m_s}{m_u} & 1 \end{bmatrix}^T \tag{5.12}$$

5.3.1 Open Loop Stability

By obtaining linearized system, now it is possible to check stability of the open loop plant. For this, eigenvalues of system matrix **A** are calculated, and they are, $\lambda_{OL} = \begin{bmatrix} 0+0i & 0+0i & 0+63.6396i & 0-63.6396i \end{bmatrix}$. Two repeating eigenvalues are located on the origin of complex plane and other two complex conjugates are located on imaginary axis, which means this system is marginally stable.

5.4 Controllability Check

A linear time invariant system is said to be completely state controllable if the controllability matrix, **M**, is full rank [54]. **M** matrix definition is:

$$\mathbf{M} = \begin{bmatrix} \mathbf{B} \vdots \mathbf{AB} \vdots \mathbf{A}^2\mathbf{B} \vdots \mathbf{A}^3\mathbf{B} \end{bmatrix} \tag{5.13}$$

For the linearized system of equation 5.5 and using system parameter values given in table 6.2, **M** is obtained as:

$$\mathbf{M} = \begin{bmatrix} 0 & 12.4195 & 0 & -50299.2636 \\ 0 & -13.4195 & 0 & 50299.2636 \\ -12.4195 & 0 & 50299.2636 & 0 \\ 1 & 0 & 0 & 0 \end{bmatrix} \tag{5.14}$$

which is a full rank matrix ($rank = 4$), therefore, the system is full state controllable.

5.5 Optimal Sliding Manifold Design

5.5.1 Weighting Matrix

The cost function equation presented in 5.4 is not suitable for optimal sliding mode motion since this motion is independent of the control and only dependent on the sliding manifold, therefore J is only function of states [36]:

$$J = \int_0^\infty [\mathbf{x}^T \mathbf{Q} \mathbf{x}] dt \tag{5.15}$$

where $\mathbf{Q}_{4\times4}$ is a positive definite matrix containing weighting factors correspond to the states that are important for the active suspension.

$$\mathbf{Q} = \begin{bmatrix} \delta_1 & 0 & 0 & 0 \\ 0 & \delta_2 & 0 & 0 \\ 0 & 0 & 0 & 0 \\ 0 & 0 & 0 & \delta_3 \end{bmatrix} \tag{5.16}$$

where:

- δ_1 is weighting factor of tire deflection.

- δ_2 is weighting factor of suspension deflection.
- δ_3 is weighting factor of sprung mass vertical speed.

5.5.2 Decomposing State Vector

The sliding surface coefficients for the controller need to be specified. This problem can be solved by using new state variables transformed from original ones, by means of a non-singular linear transformation [36],

$$\boldsymbol{\eta} = \mathbf{N}\mathbf{x} \tag{5.17}$$

such that **N** satisfies:

$$\mathbf{N}\mathbf{B} = \begin{bmatrix} 0 & 0 & 0 & b \end{bmatrix}^T \tag{5.18}$$

For doing this, the method presented in [55] is used. First, **B** is decomposed as:

$$\mathbf{B} = \begin{bmatrix} \mathbf{B}_{1_{3\times 1}} \\ \mathbf{B}_{2_{1\times 1}} \end{bmatrix} \tag{5.19}$$

where:

$$\mathbf{B}_1 = \begin{bmatrix} 0 & 0 & -\frac{m_s}{m_u} \end{bmatrix}^T \tag{5.20}$$

$$\mathbf{B}_2 = 1 \tag{5.21}$$

Then, **N** is chosen as:

$$\mathbf{N} = \begin{bmatrix} \mathbf{I}_{3\times 3} & -\mathbf{B}_1\mathbf{B}_2 \\ \mathbf{0}_{1\times 3} & \mathbf{B}_2^{-1} \end{bmatrix} \tag{5.22}$$

$$\mathbf{N} = \begin{bmatrix} 1 & 0 & 0 & 0 \\ 0 & 1 & 0 & 0 \\ 0 & 0 & 1 & \frac{m_s}{m_u} \\ 0 & 0 & 0 & 1 \end{bmatrix} \tag{5.23}$$

And the new state space is:

$$\boldsymbol{\eta} = \begin{bmatrix} x_1 & x_2 & x_3 + \frac{m_S}{m_u}x_4 & x_4 \end{bmatrix}^T \tag{5.24}$$

$$\dot{\boldsymbol{\eta}} = \mathbf{N}\mathbf{A}\mathbf{N}^{-1}\boldsymbol{\eta} + \mathbf{N}\mathbf{B}u \tag{5.25}$$

$$\dot{\boldsymbol{\eta}} = \mathbf{A}_N\boldsymbol{\eta} + \mathbf{B}_N u \tag{5.26}$$

$\mathbf{A}_N$ is decomposed to four sub-matrices,

$$\mathbf{A}_N = \begin{bmatrix} \mathbf{A}_{N_{11}} & \mathbf{A}_{N_{12}} \\ \mathbf{A}_{N_{21}} & \mathbf{A}_{N_{22}} \end{bmatrix} \tag{5.27}$$

The state vector $\boldsymbol{\eta}$, decomposed into two sub systems consisting of three states $\mathbf{x}_1 = \begin{bmatrix} \eta_1 & \eta_2 & \eta_3 \end{bmatrix}$, and one element of it $x_2 = \eta_4$.

$$\dot{\mathbf{x}}_1 = \mathbf{A}_{N_{11}}\mathbf{x}_1 + \mathbf{A}_{N_{12}}x_2 \tag{5.28}$$

$$\dot{x}_2 = \mathbf{A}_{N_{21}}\mathbf{x}_1 + \mathbf{A}_{N_{22}}x_2 + bu \tag{5.29}$$

where:

$$\mathbf{A}_{N_{11}} = \begin{bmatrix} 0 & 0 & -1 \\ 0 & 0 & 1 \\ \frac{k_t}{m_u} & 0 & 0 \end{bmatrix} \tag{5.30}$$

$$\mathbf{A}_{N_{12}} = \begin{bmatrix} \frac{m_s}{m_u} \\ -\frac{m_s}{m_u} - 1 \\ 0 \end{bmatrix} \tag{5.31}$$

$$\mathbf{A}_{N_{21}} = \begin{bmatrix} 0 & 0 & 0 \end{bmatrix} \tag{5.32}$$

$$\mathbf{A}_{N_{22}} = [0] \tag{5.33}$$

and $b = 1$. So, the decomposed subsystems are:

$$\dot{\mathbf{x}}_1 = \mathbf{A}_{N_{11}}\mathbf{x}_1 + \mathbf{A}_{N_{12}}x_2 \tag{5.34}$$

$$\dot{x}_2 = u \tag{5.35}$$

5.5.3 Optimal Sliding Manifold

Sliding surface for the decomposed system of 5.34 is assumed to be [36]:

$$S = \mathbf{S}_0\mathbf{x}_1 + x_2 \tag{5.36}$$

where the elements of the $\mathbf{S}_0$ matrix, i.e. the coefficients of the sliding surface are specified such that the cost function J is minimized. Also, the transformed weighting

matrix $\mathbf{Q}$ is:

$$\mathbf{Q}_N = (\mathbf{N}^{-1})^T \mathbf{Q} \mathbf{N}^{-1} \tag{5.37}$$

$$\mathbf{Q}_N = \begin{bmatrix} \mathbf{Q}_{N_{11}} & \mathbf{Q}_{N_{12}} \\ \mathbf{Q}_{N_{21}} & \mathbf{Q}_{N_{22}} \end{bmatrix} \tag{5.38}$$

where:

$$\mathbf{Q}_{N_{11}} = \begin{bmatrix} \delta_1 & 0 & 0 \\ 0 & \delta_2 & 0 \\ 0 & 0 & 0 \end{bmatrix} \tag{5.39}$$

$$\mathbf{Q}_{N_{12}} = \begin{bmatrix} 0 \\ 0 \\ 0 \end{bmatrix} \tag{5.40}$$

$$\mathbf{Q}_{N_{12}} = \begin{bmatrix} 0 & 0 & 0 \end{bmatrix} \tag{5.41}$$

$$\mathbf{Q}_{N_{22}} = [\delta_3] \tag{5.42}$$

After transformation, the cost function presented in equation 5.15 is:

$$J = \int_0^\infty \boldsymbol{\eta}^T \mathbf{Q}_N \boldsymbol{\eta} \, dt \tag{5.43}$$

$$J = \int_0^\infty \left[\mathbf{x}_1^T \mathbf{Q}_{N_{11}} \mathbf{x}_1 + \mathbf{Q}_{N_{22}} x_2^2 \right] dt \tag{5.44}$$

In sliding motion on the sliding manifold $S = 0$, only values of vector $\mathbf{x}_1$ is obtained and x_2 is obtained from:

$$x_2 = -\mathbf{S}_0 \mathbf{x}_1 \tag{5.45}$$

The $\mathbf{S}_0$ is obtained as [36]:

$$\mathbf{S}_0 = \mathbf{Q}_{N_{22}}^{-1} \mathbf{A}_{N_{12}}^T P \tag{5.46}$$

where $\mathbf{P}$ is the unique solution of the matrix Riccati equation:

$$\mathbf{P}\mathbf{A}_{N_{11}} + \mathbf{A}_{N_{11}}^T \mathbf{P} - \mathbf{P}\mathbf{A}_{N_{12}} \mathbf{Q}_{N_{22}}^{-1} \mathbf{A}_{N_{12}}^T \mathbf{P} + \mathbf{Q}_{N_{11}} = 0 \tag{5.47}$$

and finally the coefficients matrix of the optimal sliding surface $\mathbf{C}_{1\times 4}$, presented in equation 5.1, is:

$$\mathbf{C} = \left[\mathbf{Q}_{N_{22}}^{-1} \mathbf{A}_{N_{12}}^T P \quad 1 \right] \mathbf{N} \tag{5.48}$$

5.5.4 Eigenvalues of Sliding Mode Equation

Motion of states on the sliding surface $S = 0$ is defined by equation 5.45. By substituting equation 5.45 in equation 5.34 the ODE for the sliding mode motion is obtained as:

$$\dot{\mathbf{x}}_1 = \big(\mathbf{A}_{N_{11}} - \mathbf{A}_{N_{12}}\mathbf{S}_0\big)\mathbf{x}_1 \tag{5.49}$$

If the eigenvalues of the new system matrix $(\mathbf{A}_{N_{11}} - \mathbf{A}_{N_{12}}\mathbf{S}_0)$, all have negative real parts, then it means sliding motion is stable [36].

5.6 Control Law Design

5.6.1 Linearized Control Input

Normally a sign function is suggested for control law [36] which regulates the state trajectory in sliding motion to keep it on the sliding manifold, but it causes chattering problem. To prevent any chattering problem, a smooth tangent hyperbolic function is used, which has a similar behavior of sign function but with the advantage of being continuous and differentiable [51].

$$u = -U \tanh \frac{S}{\epsilon} \tag{5.50}$$

where:

$$U \geq 0 \tag{5.51}$$

$$\epsilon \simeq 0 \tag{5.52}$$

U is the control gain. And ϵ is for amplifying the argument of tangent hyperbolic function to make its behavior similar to sign function.

5.6.2 De-linearization of control Input

u is the linearized control input. It has the original non-linear control input F_a, in it. So after rearranging, F_a is obtained as:

$$F_a = u\, m_s + k_{1s}(d_{s0} - x_2) + k_{2s}(d_{s0} - x_2)^3 + m_s g + c_S(x_4 - x_3) \tag{5.53}$$

5.7 Lyapunov Stability Analysis

For proving the Lyapunov stability of the system expressed by equations 5.5, an invariant transformation is done. This has no effect on system dynamics and the sliding mode control applied [36]. The sliding surface S is transformed to the new one S^* as follows:

$$S^* = \mathbf{\Omega} S \tag{5.54}$$

where:

$$\mathbf{\Omega} = (\mathbf{CB})^{-1} \tag{5.55}$$

with $\mathbf{C}_{1\times4}$ containing the sliding surface coefficients and $\mathbf{B}_{4\times1}$ is the control input matrix. After this transformation, the time derivative of the new sliding surface can be written as:

$$\dot{S}^* = \mathbf{\Omega}\dot{S} \tag{5.56}$$

$$\dot{S}^* = \mathbf{\Omega C}\dot{\mathbf{x}} \tag{5.57}$$

$$\dot{S}^* = \mathbf{\Omega C}\big(\mathbf{Ax} + \mathbf{B}u\big) \tag{5.58}$$

$$\dot{S}^* = \mathbf{\Omega CAx} + \mathbf{\Omega CB}u \tag{5.59}$$

$$\dot{S}^* = \mathbf{\Omega CAx} + u \tag{5.60}$$

$$\dot{S}^* = \mathbf{Ex} + u \tag{5.61}$$

where:

$$\mathbf{E} = \mathbf{\Omega CA} \tag{5.62}$$

The sliding mode controller can be written as:

$$u = -U\,\mathrm{sgn}(S) \tag{5.63}$$

And for stability, The Lyapunov function is chosen as:

$$V = \frac{1}{2}S^{*2} \tag{5.64}$$

Time derivative of this Lyapunov function can be written as:

$$\dot{V} = S^*\dot{S}^* \tag{5.65}$$

$$= S^*\big(\mathbf{Ex} + u\big) \tag{5.66}$$

$$= S^*\big(\mathbf{Ex} - U\,\mathrm{sgn}(S)\big) \tag{5.67}$$

$$= S^*\,\mathrm{sgn}(S)\big(\,\mathrm{sgn}(S)\mathbf{Ex} - U\big) \tag{5.68}$$

From equation 5.68 it can be seen that:

$$\dot{V} \leq |S^*|\Big(|\mathbf{Ex}| - U\Big) \tag{5.69}$$

For a positive constant K value that satisfies:

$$\dot{V} \leq -K|S^*| \tag{5.70}$$

The following equation that satisfies stability can be written:

$$|\mathbf{Ex}| - U \leq -K \tag{5.71}$$

or:

$$U \geq |\mathbf{Ex}| + K \tag{5.72}$$

For satisfying equation 5.72, U is chosen as follows:

$$U = |\mathbf{Ex}|_{max} + K \tag{5.73}$$

5.8 State Estimator

5.8.1 Observability of the Non-linear System

Th observability of the non-linear system can be checked in a similar way that was done in chapter 3. That matrix **O** should be full rank.

$$\mathbf{O} = \frac{\partial \mathbf{G}}{\partial \mathbf{x}} \tag{5.74}$$

where **G** matrix is a combination of all successive Lie derivations of output function vector **h**, with respect to system vector **f**:

$$\mathbf{G} = \begin{bmatrix} L_f^0\mathbf{h} & L_f^1\mathbf{h} & L_f^2\mathbf{h} & L_f^3\mathbf{h} \end{bmatrix} \tag{5.75}$$

The rank of $\mathbf{O}_{8\times4}$ matrix should be evaluated for all values of the operating points in the entire duration of the simulation. The rank is calculated and plotted in figure 5.1. As seen in this figure, rank is always 4, which means the system is locally observable for the entire duration of the simulation. Therefore it is possible to design a non-linear observer for the system of this study.

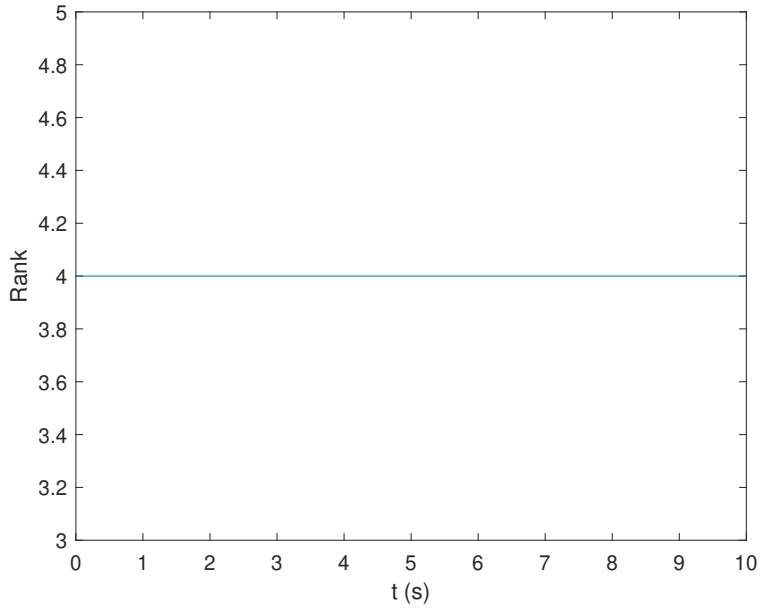

Figure 5.1: Rank of observability matrix $\mathbf{O}_{8\times4}$ for all time steps

5.8.2 Extended Kalman Filter

As discussed earlier, an extended Kalman filter is used for estimating states from outputs, which are sprung and unsprung mass accelerations. The state equations are discretized as follows:

$$\hat{\mathbf{x}}_{k+1} = \hat{\mathbf{x}}_k + \tau\big(\mathbf{f}(\hat{\mathbf{x}}_k) + \mathbf{B}F_{a_{k-1}}\big) \tag{5.76}$$

where τ is time step of discretization and $\hat{\mathbf{x}}$ is estimated states vector. Non-linear terms should be linearized using Taylor series:

$$\mathbf{F}(\hat{\mathbf{x}}, k) = \frac{\partial \hat{\mathbf{x}}_{k+1}}{\partial \mathbf{x}}\Big|_{\mathbf{x}=\hat{\mathbf{x}}_{k|k}} \tag{5.77}$$

$$\mathbf{H}(\hat{\mathbf{x}}, k) = \frac{\partial \mathbf{h}}{\partial \mathbf{x}}\Big|_{\mathbf{x}=\hat{\mathbf{x}}_{k|k-1}} \tag{5.78}$$

$\mathbf{W}$ and $\mathbf{V}$ matrices, using equations 3.17 and 3.18 are:

$$\mathbf{W} = \frac{\partial \hat{\mathbf{x}}_{k+1}}{\partial \omega} = \begin{bmatrix} tau & 0 & 0 & 0 \end{bmatrix}^T \tag{5.79}$$

$$\mathbf{V} = \frac{\partial \mathbf{y}}{\partial v} = \mathbf{I} \tag{5.80}$$

Extended Kalman filter procedure was already described in chapter 3. The only difference now is F_a term that shows up in the equations and d_{s0} is not a state anymore,

its value is constant that was estimated prior to the activating the controller. Extended Kalman filter algorithm for discrete system is:

1. State prediction based on previous estimated state:

$$\hat{\mathbf{x}}_{k|k-1} = \hat{\mathbf{x}}_{k-1|k-1} + \tau\ \mathbf{f}(\hat{\mathbf{x}}_{k-1|k-1}) + \tau\ \mathbf{B} F_{a_{k-1}} \tag{5.81}$$

2. Prediction of estimation error covariance:

$$\mathbf{P}_{k|k-1} = \mathbf{F}_{k-1|k-1}\ \mathbf{P}_{k-1|k-1}\ \mathbf{F}^{T}_{k-1|k-1} + \mathbf{W}\ \mathbf{Q}\ \mathbf{W}^{T} \tag{5.82}$$

3. Computing Kalman gain:

$$\mathbf{K}_k = \mathbf{P}_{k|k-1}\ \mathbf{H}^{T}_{k|k-1} \Big[\mathbf{H}_{k|k-1}\ \mathbf{P}_{k|k-1}\ \mathbf{H}^{T}_{k|k-1} + \mathbf{R}\Big]^{-1} \tag{5.83}$$

4. Updating estimated states with measurements from current step:

$$\hat{\mathbf{x}}_{k|k} = \hat{\mathbf{x}}_{k|k-1} + \mathbf{K}_k \Big(\mathbf{y}_k - \mathbf{h}(\hat{\mathbf{x}}_{k|k-1}) - \mathbf{D} F_{a_k}\Big) \tag{5.84}$$

5. Updating estimation error covariance:

$$\mathbf{P}_{k|k} = \mathbf{P}_{k|k-1} - \mathbf{K}_k\ \mathbf{H}_{k|k-1}\ \mathbf{P}_{k|k-1} \tag{5.85}$$

In equations above, $\mathbf{Q}$ is process noise covariance and $\mathbf{R}_{2\times 2}$ is measurements noise covariance matrix:

$$\mathbf{Q} = Q_1 \tag{5.86}$$

$$\mathbf{R} = \begin{bmatrix} R_1 & 0 \\ 0 & R_2 \end{bmatrix} \tag{5.87}$$

where Q_1 is road profile speed covariance and R_1 and R_2 are unsprung mass accelerometer and sprung mass accelerometer noise covariances respectively.

CHAPTER 6

SIMULATION

6.1 Simulation Models

In this chapter simulation procedure is described. System model is designed by Matlab-Simulink software. There are three different models in this study:

- Passive Suspension, which is the base conventional model without the controller. Parameter estimation is carried out in this model.
- Active Suspension with Optimal Sliding Mode Control.
- Active Suspension with Improved Optimal Sliding Mode Control [17].

Simulations for investigating performance of parameter estimator and effect of using incorrect sprung mass in designing the OSMC is carried out for three different values of sprung mass. These three cases are given in table 6.1. In the following sections, all sub-systems of the models are described and the parameters used in the simulation are presented.

Table 6.1: Cases of sprung mass for simulation

Vehicle	$m_s(kg)$	$d_{s0}(m)$
Unloaded	1241.78	-0.15092
Half-loaded	1444.59	-0.175
Full-loaded	1657.08	-0.2

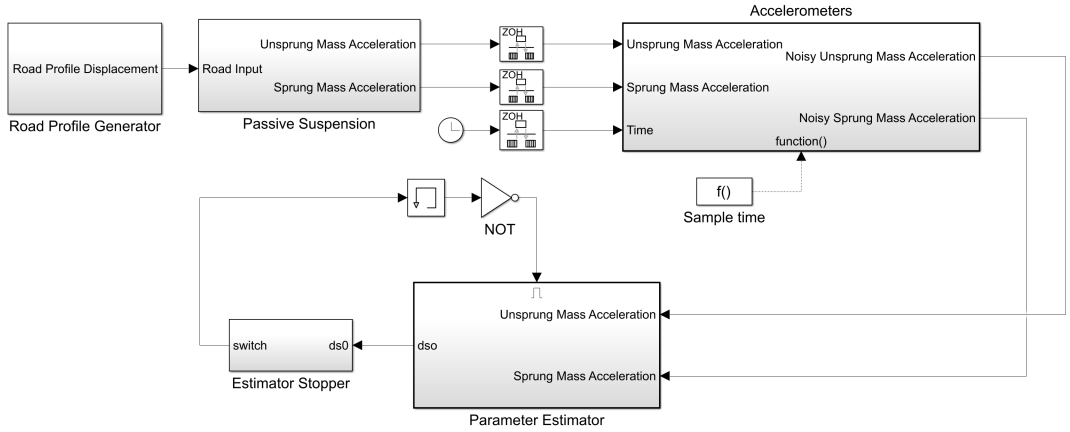

Figure 6.1: Block diagram of passive suspension with parameter estimator

6.1.1 Passive Model with Parameter Estimator

The Simulink block diagram for the passive suspension model is presented in figure 6.1. "Passive Suspension" sub-system is built based on equations 3.12 and 3.13 (figure A.1). The disturbance of this sub-system is road profile z_r. Displacement and speed of sprung and unsprung masses is obtained by integrating the accelerations. The outputs of this sub-system are fed into an accelerometer model which is described in section 6.4.

Parameter estimation is done on the passive system. The output of the accelerometer sub-system; i.e. the acceleration measurement signals are fed into the EKF parameter estimator sub-system to estimate $\hat{d}_{s0}$. The estimated $\hat{d}_{s0}$ value is used in the controller sub-system. The control algorithm that runs in this sub-system was explained in chapter 5.

6.1.2 Active Suspension with OSMC

The block diagram of this model is presented in figure 6.2. The "Active Suspension" sub-system is built based on equations 3.29 and 3.30 (figure A.2). Road profile z_r, is the disturbance and F_a is the control input of the active suspension sub-system. Outputs are sprung and unsprung mass accelerations, $\ddot{z}_s$ and $\ddot{z}_u$. These measurement

signals are fed into the EKF state estimator to estimate states which are fed into to "OSMC" sub-system that generates the required control action u. This linearized control signal is fed into the de-linearization sub-system to obtain the actual control input F_a. By means the control loop is closed.

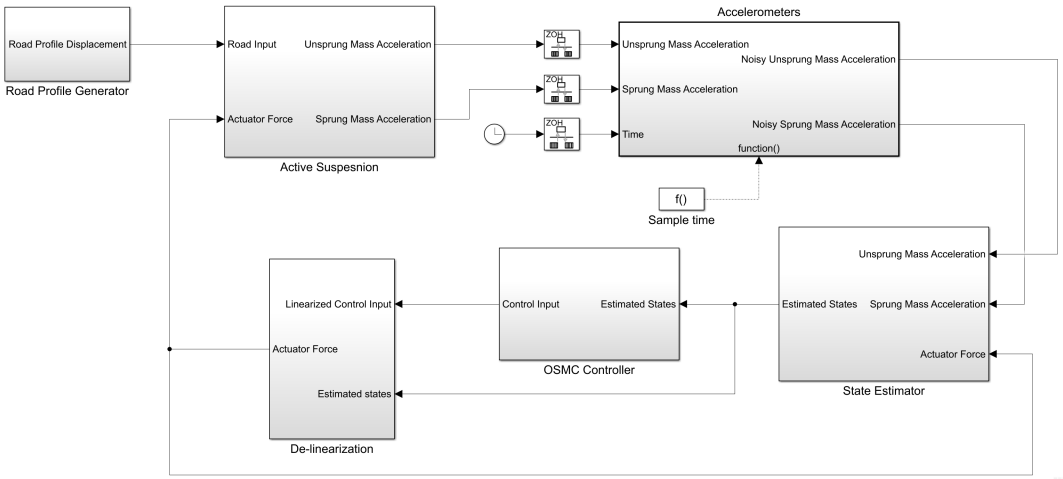

Figure 6.2: Block diagram of active suspension with OSMC

6.1.3 Active Suspension with IOSMC

The block diagram of this model is presented in figure 6.3. This model uses the IOSMC approach described in [17] instead of OSMC. The Simulink model for the plant is the same which is presented in figure A.2. This controller is discussed in section 6.8.

6.2 Model Parameters

Parameters used for the quarter car model are presented in table 6.2. The simulation parameters on the hand, are given in table 6.4.

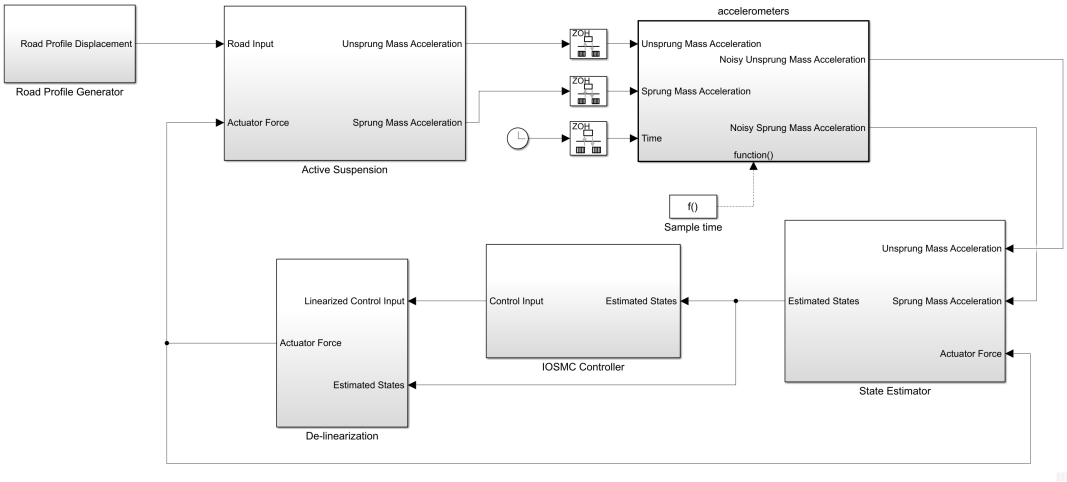

Figure 6.3: Block diagram of active suspension with IOSMC

Table 6.2: Vehicle parameters

Parameter	Sign	Unit	Value
Sprung Mass	m_s	kg	1242
Unsprung Mass	m_u	kg	100
Linear Spring Stiffness Coefficient	k_{1s}	$\frac{N}{m}$	80000
Non-linear Spring Stiffness Coefficient	k_{2s}	$\frac{N}{m}$	32000
Upward Damping Coefficient	c_{1s}	$\frac{N.s}{m}$	4000
Downdward Damping Coefficient	c_{2s}	$\frac{N.s}{m}$	1600
Damping Coefficients Difference	Δc_s	$\frac{N.s}{m}$	775
Damping Coefficients Average	$\bar{c}_s$	$\frac{N.s}{m}$	2800
Tire Stiffness Coefficient	k_t	$\frac{N}{m}$	405000
Max Actuator Force	F_a	N	2100
Vehicle Longitudinal speed	V	$\frac{m}{s}$	20
Suspension static Deflection	d_{s0}	m	-0.1590
Tire static Deflection	d_{t0}	m	-0.0325

6.3 Road Profile Generation

The disturbance in all models, is road profile. Road surfaces are not even, they have irregularities. These irregularities act as the disturbance to the suspension system. The road profile can be modeled by a step or a sinusoidal function. However, actual road surfaces are not deterministic. Modeling the road profile as a random process is more accurate and is the approach used in active suspension control literature [56].

6.3.1 ISO-8608 Road Classification

According to [57], road profile can be treated as a Gaussian random process. Its power spectral density is classified by the degree of roughness. The so called spatial frequency (6.1) is used in defining the power spectral density. It can be formulated as:

$$\Omega = \frac{\omega}{V} \quad (\frac{rad}{m}) \tag{6.1}$$

where ω is angular frequency and V is vehicle longitudinal speed. By means the PSD of the road profile can be represented as:

$$G_d(\Omega) = G_d(\Omega_0)(\frac{\Omega}{\Omega_0})^{-w} \tag{6.2}$$

where w is waviness number and is taken as 2 and Ω_0 is the reference angular spatial frequency taken as 1 $(\frac{rad}{m})$. $G_d(\Omega_0)$ takes different values, depending on the road roughness level as shown, in table 6.3. Therefore A class road profile represents a smooth road profile and H class represents a very rough road surface. The PSD for these different classes of roads is shown in 6.4. B class road profile is considered for the simulations performed in this work as it represents a relatively smooth road profile like asphalt roads.

Table 6.3: Road classification – ISO 8608

Road Class	Lower Limit	Geometric Mean	Upper Limit
	Degree of Road Roughness $G_d(\Omega_0)10^{-6}(\frac{m^3}{rad})$		
A	-	1	2
B	2	4	8
C	8	16	32
D	32	64	128
E	128	256	512
F	512	1024	2048
G	2048	4096	8192
H	8192	16384	-

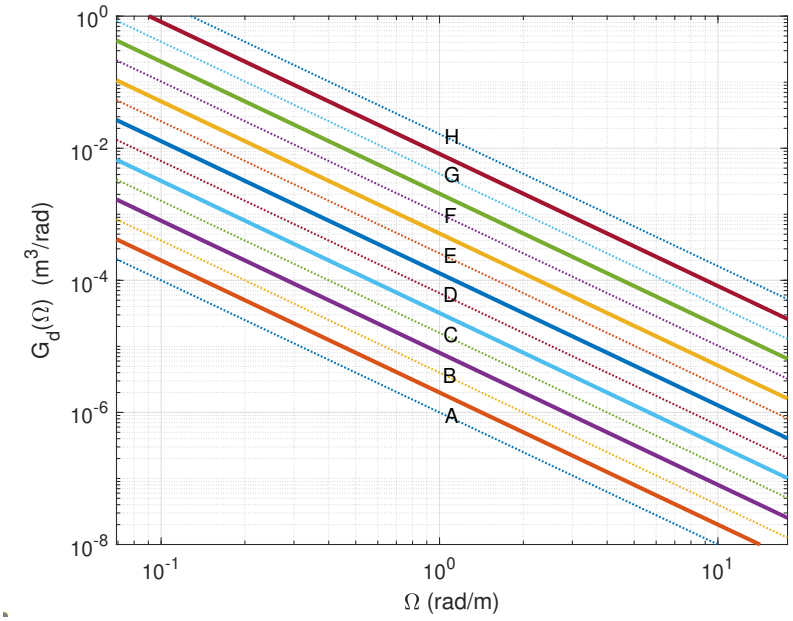

Figure 6.4: Road classification by ISO-8608

6.3.2 Shape Filtering

6.3.2.1 Reason of Usage

Area under the PSD diagram is equal to the variance of process. However, as observable from the figure 6.4:

$$\lim_{\Omega \to 0} G_d(\Omega) \to \infty \tag{6.3}$$

In other words the variance and the PSD of the road profile would go to infinity, at zero spatial frequency. Therefore, the PSD expression is modified as [58, 59]:

$$G_d(\Omega) = \frac{2\alpha\sigma^2}{\alpha^2 + \Omega^2} \quad (\frac{m^3}{rad}) \tag{6.4}$$

which is a one-sided PSD of road profile and α is road roughness parameter with the unit of $(\frac{rad}{m})$ and σ is road profile standard deviation with the unit of (m^2).

6.3.2.2 Calculating Parameters

For calculating σ, upper and lower spatial angular frequency range should be defined. In ISO-8608 values for lower and upper limits are suggested as $\Omega_1 = 0.022\pi$ and $\Omega_N = 5.66\pi$. So, by using equation 6.2, σ can be calculated as [59]:

$$\sigma^2 = \frac{1}{2\pi}\int_0^\infty G_d(\Omega)d\Omega \tag{6.5}$$

$$= \frac{G_d(\Omega_0)}{2\pi}(\frac{2}{\Omega_1} - \frac{1}{\Omega_N}) \tag{6.6}$$

By substituting all constant values except the $G_d(\Omega_0)$, variance is:

$$\sigma^2 = 4.5966\ G_d(\Omega_0) \tag{6.7}$$

and the standard deviation value obtained as $\sigma = 0.0043\ (m^2)$ for B class road profile. For obtaining α the value of PSD in equation 6.4 should be evaluated in Ω_0 [59]:

$$G_d(\Omega_0) = \frac{2\alpha 4.5966 G_d(\Omega_0)}{\alpha^2 + \Omega_0^2} \tag{6.8}$$

It shows that value of α is independent of road class. Finally we obtain, $\alpha = 0.1101 \quad \frac{rad}{m}$.

6.3.2.3 PSD of White Noise

Since the relation between spatial angular frequency (Ω) and temporal angular frequency (ω) is [59]:

$$G_d(\omega) = \frac{G_d(\Omega)}{V} \tag{6.9}$$

Equation 6.4 can be rewritten in angular frequency ω domain:

$$G_d(\omega) = \frac{2\alpha V\sigma^2}{\alpha^2 V^2 + \omega^2} \quad (\frac{m^2}{\frac{rad}{s}}) \tag{6.10}$$

It is actually a frequency response of a low pass filter to white noise with a constant PSD of $G_d(w) = 2\alpha V\sigma^2$.

6.3.2.4 Time Domain Response

If the vehicle runs with constant velocity V, then the road profile signal, $z_r(t)$, whose PSD is given by equation 6.10, may be obtained as the output of a linear filter expressed by the differential equation:

$$z_r(t) = -\alpha V z_r(t) + w(t) \tag{6.11}$$

where $w(t)$ is a white noise with the constant PSD of $G_d(w) = 2\alpha V\sigma^2 \quad (\frac{rad.m^2}{s})$.

6.3.2.5 White Noise Standard Deviation

For generation of road profile in time domain zero mean white noise should pass through the equation 6.11. As mentioned before, standard deviation is square root of the area under PSD plot for a specific temporal frequency range. Therefore, it can be represented as:

$$\sigma_w = \sqrt{G_d(w)(\omega_N - \omega_1)} \tag{6.12}$$

Where $\omega_1 = 0.022\pi V$ and $\omega_N = 5.660\pi V$ and it is obtained as $\sigma_w = 0.1694 \quad (\frac{rad^2m^2}{s^2})$.

6.3.2.6 Generating of Time Domain Road Profile

Vehicle constant longitudinal speed is $20\ (\frac{m}{s})$, therefore maximum road frequency of interest is $f_N = 56.6\ (Hz)$. For the sake of a taking wider range of frequencies, it

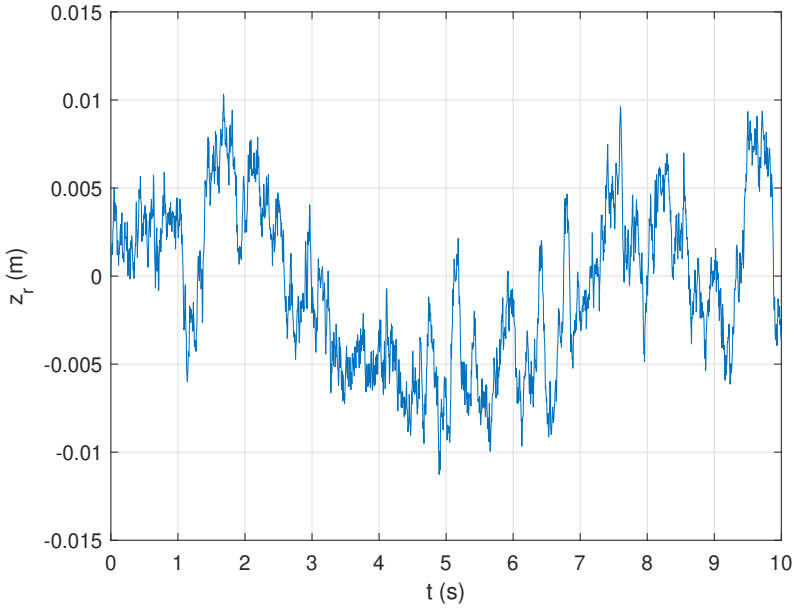

Figure 6.5: Road profile in time domain

is taken as $100\ (Hz)$. Since, sampling frequency is twice maximum frequency [60], white noise is sampled at $f_s = 200\ (Hz)$. Therefore, sampling rate is:

$$\Delta t = \frac{1}{f_s} \rightarrow \Delta t = 0.005\ (s) \tag{6.13}$$

Sampling is done considering a duration of $10\ (s)$. "Road Profile Generator" sub-system is presented in figure A.3. The road profile generated for B class road at the speed of $20\ \left(\frac{m}{s}\right)$ is given in figure 6.5. On the other hand, figure 6.6 shows the PSD of the random road profile transformed to frequency domain. In the same figure, the PSD of the B class road profile alongside its upper and lower limits is also plotted. The green and the purple curves, match as expected.

6.4 Accelerometers

The sub-system for accelerometer model is shown in A.4. Gaussian white noise is added to sprung and unsprung mass accelerations. The covariances of the measurement noises were presented in table 6.4. Figure 6.7 shows the sprung mass acceleration signal with and without added noise.

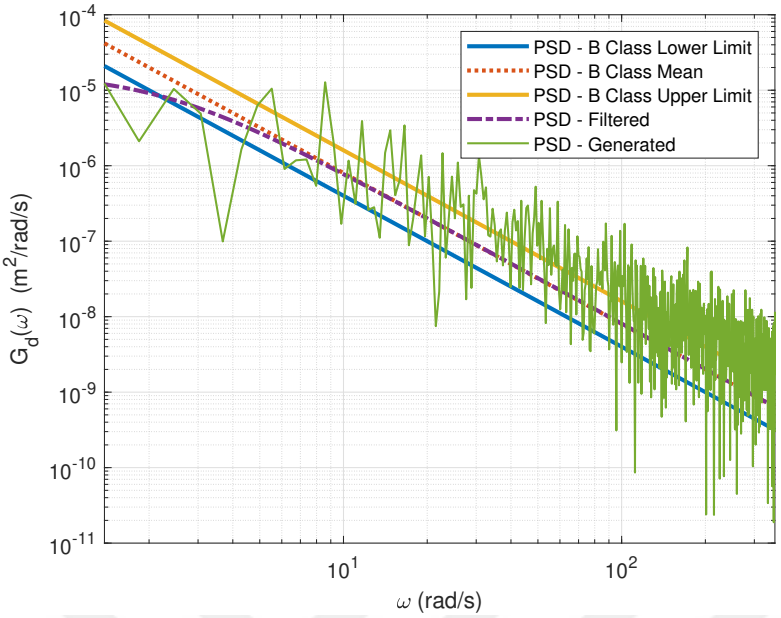

Figure 6.6: PSD lines of road profile class B

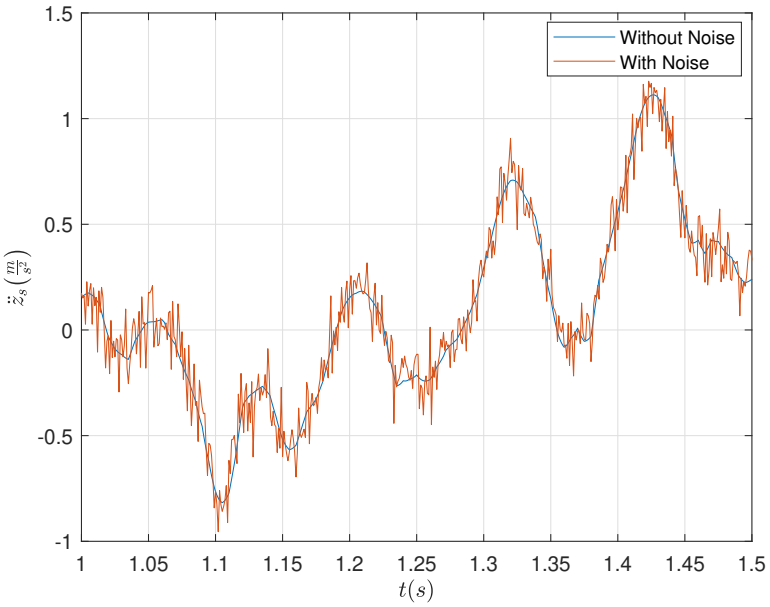

Figure 6.7: Additive noise on sprung mass acceleration

6.5 Parameter Estimator and its Stopper

Figure A.5 shows the "Parameter Estimator" sub-system. In this sub-system measured sprung and unsprung mass accelerations, are fed into the EKF block responsible for state estimation. The state of interest here is the fifth state d_{s0}. Estimation error covariances are among the outputs of this block. The estimation is concluded based on the following criteria:

First the values of $\hat{d}_{s0}$ for which the estimation error covariance P_{55} is less than 1×10^{-5} are collected. This is done in "Parameter Estimator" sub-system shown in figure A.5.

Then in the "Parameter Estimator Stopper" sub-system shown in figure A.6 the standard deviation for the 100 consecutive $\hat{d}_{s0}$ elements is computed. The estimation is concluded when the standard deviation for these 100 elements is less than 1×10^{-6}. Initial values of the states and estimation error covariance used in the EKF block are:

$$X_0 = \begin{bmatrix} 0 & 0 & 0 & 0 & -0.2 \end{bmatrix}^T \tag{6.14}$$

$$P_0 = \begin{bmatrix} 0.01 & 0 & 0 & 0 & 0 \\ 0 & 0.01 & 0 & 0 & 0 \\ 0 & 0 & 0.01 & 0 & 0 \\ 0 & 0 & 0 & 0.01 & 0 \\ 0 & 0 & 0 & 0 & 0.01 \end{bmatrix} \tag{6.15}$$

6.6 State Estimator

State estimator sub-system is very similar to the "parameter Estimator" sub-system. Measured sprung and unsprung mass accelerations are discretized and fed to extended Kalman filter block which estimates all 4 states shown in equation 3.15. This sub-system is shown in figure A.7. Actuator force F_a and $\hat{d}_{s0}$ are also inputs of this sub-system. Initial values of the states and estimation error covariance used in the

Table 6.4: Simulation parameters

Parameter	Value
Simulation duration	$10\ (s)$
Simulation Time Step	$0.1\ (ms)$
Accelerometer Time Step	$1\ (ms)$
Estimators Time Step	$1\ (ms)$
Unsprung Mass Accelerometer Noise Covariance, R_1	0.1
Sprung Mass Accelerometer Noise Covariance, R_2	0.01
Road Profile Speed Covariance, Q_1	9×10^{-4}
d_{s0} Variation Covariance, Q_5	1×10^{-8}

EKF block are:

$$X_0 = \begin{bmatrix} 0 & 0 & 0 & 0 \end{bmatrix}^T \tag{6.16}$$

$$P_0 = \begin{bmatrix} 0.01 & 0 & 0 & 0 \\ 0 & 0.01 & 0 & 0 \\ 0 & 0 & 0.01 & 0 \\ 0 & 0 & 0 & 0.01 \end{bmatrix} \tag{6.17}$$

6.7 OSMC Controller

Figure A.8 shows "OSMC Controller" sub-system. As it is stated in section 5.7, if U satisfies equation 5.73, the closed loop system is stable. For this reason, the value of $|\mathbf{Ex}|$ is calculated and plotted in figure 6.8. Maximum value of the $|\mathbf{Ex}|$ is 1.2. Therefore, if U is chosen higher than 1.2, the closed-loop system would be stable. The value of the control gain U, weighting factors and sliding surface coefficients C are given in table 6.5.

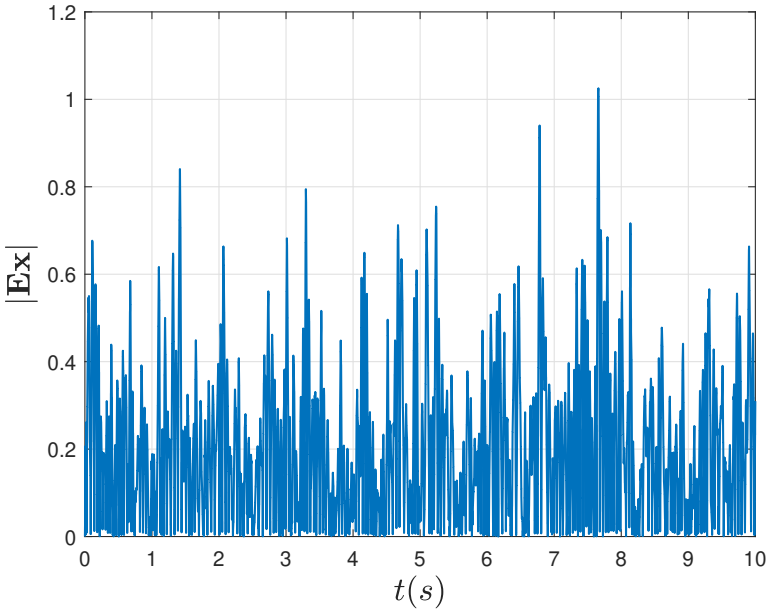

Figure 6.8: Value of |**Ex**| for entire duration of simulation

Table 6.5: OSMC parameters

Parameter	Value
U	50
ϵ	$\frac{1}{3}$
δ_1	35689
δ_2	27862
δ_3	10000
C	0.851642 -1.669191 0.000350 1.004378

6.8 IOSMC controller

This controller is the one proposed in [17]. The sub-system showing the model of this controller is shown in A.9. In this method, the sprung mass acceleration, expressed by U, is added as the 5th state:

$$\mathbf{x}_1 = \begin{bmatrix} x_1 & x_2 & x_3 & x_4 & U \end{bmatrix}^T \tag{6.18}$$

where:

$$x_1 = z_u - z_r \tag{6.19a}$$

$$x_2 = z_s - z_u \tag{6.19b}$$

$$x_3 = \dot{z}_u \tag{6.19c}$$

$$x_4 = \dot{z}_s \tag{6.19d}$$

Sprung mass acceleration is expressed as a function of the artificial input U_a, as follows:

$$\dot{U} = a\,U + b\,U_a \tag{6.20}$$

where:

$$U_a = -\mathbf{G}\mathbf{x}_1 \tag{6.21}$$

$$\mathbf{G} = (\mathbf{K}_a\mathbf{B}_1)^{-1}(\mathbf{K}_a\mathbf{A}_1 + \lambda_a\mathbf{K}_a) \tag{6.22}$$

$\mathbf{K}_{a_{1\times 5}}$ is sliding surface coefficients matrix, $\mathbf{A}_1$ is the augmented systems matrix and $\mathbf{B}_1$ is the augmented system control input matrix. The mathematical proof and the procedure of obtaining the control law and the sliding surface can be found in [17]. The values of control parameters are presented in table 6.6.

Table 6.6: IOSMC parameters

Parameter	Value
λ_a	1
a	1
b	0.001
δ_1	35689
δ_2	2786
R	1
$\mathbf{G}$	-11371139 -52782 82786 -63479 -47881

6.9 De-linearization

The sub-system responsible for de-linearization of the control input for both OSMC and IOSMC is shown in figure A.10. This sub-system is basically responsible for applying equation 5.53. A saturation block is also placed in this sub-system that limits the maximum actuator force with it maximum force capacity (table 6.2).

6.10 ISO 2631 Frequency Weighting

As mentioned before, the main criteria in evaluating passenger ride comfort is sprung mass acceleration. ISO-2631 [1] gives a band pass filter for filtering the sprung mass acceleration whose frequency response function is shown in figure 6.9.

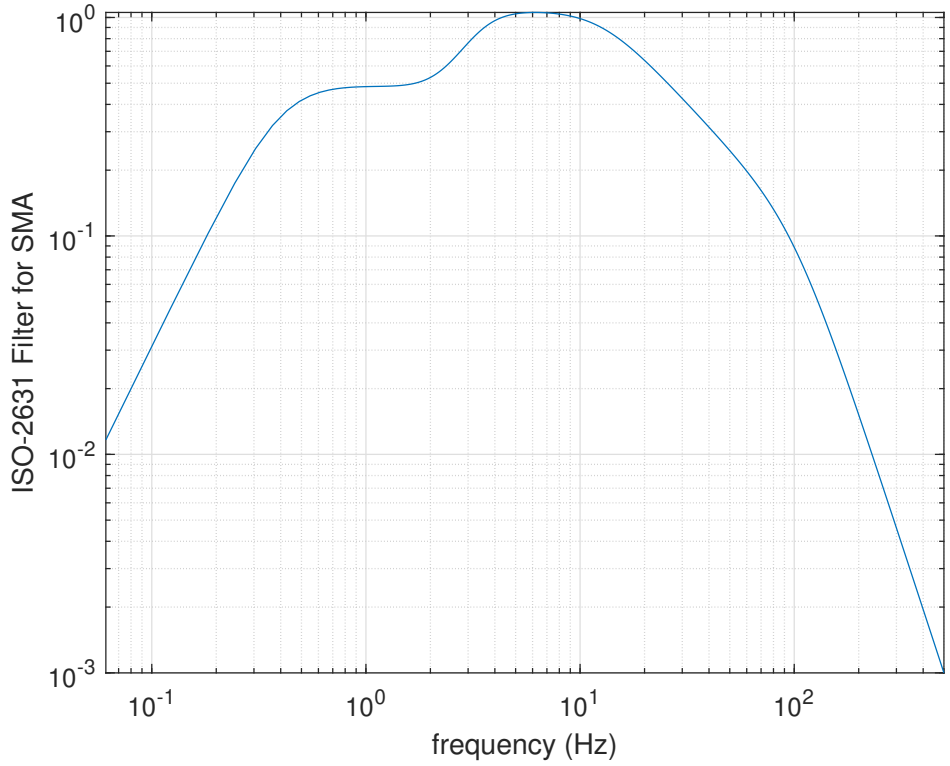

Figure 6.9: Frequency weighting curve

The filter, has a band-pass range of $4 - 9$ Hz, the critical frequency range for human body. The equations and constants for deriving this filter is provided in appendix B.

6.10.1 Ride Comfort Criterion

After obtaining the RMS value of the sprung mass acceleration it can be compared by the following values from ISO-2631.

Table 6.7: ISO-2631 comfort criteria

Sprung Mass Acceleration RMS $\left(\frac{m}{s^2}\right)$	Level of Discomfort
< 0.315	Not uncomfortable
$0.315 - 0.63$	A little uncomfortable
$0.5 - 1$	Fairly uncomfortable
$0.8 - 1.6$	Uncomfortable
$1.25 - 2.5$	Very uncomfortable
$2 <$	Extremely uncomfortable

CHAPTER 7

RESULTS & CONCLUSION

7.1 Non-linear Consideration of Spring

As it is discussed in section 2.5, spring has a non-linear behavior, but for small deflections, it can be considered as linear. Taking spring linear or non-linear may effect response of the suspension. This difference is investigated for passive suspension with simulations and the results are presented here. Simulation done for two cases of linear and non-linear spring. In each case 3 different road profiles are used, road profile class B, C, D and E to present rough road profiles. All other inputs and parameters are same in the simulations. Spring force presented in 3.1. In this equation, by taking $k_{2s} = 0$, spring becomes linear. So, the non-linear spring force equation is equation 3.1 and the linear spring force equation is:

$$F_S(d_{s0} + z_s - z_u) = k_{1s}(d_{s0} + z_s - z_u) \tag{7.1}$$

After doing the simulation, results are presented in table 7.1. This table shows only ISO-2631 filtered sprung mass acceleration RMS value since it is the main criteria for ride comfort. As table shows, absolute value of the change in sprung mass acceleration increases as the road gets rougher. This change is actually the loss of accuracy in the suspension response.

For the road class B used in this study, the change is less than $1\ \%$. So, this change can be neglected and the spring can be considered as linear for this road class. But, for the cases of rougher road profiles, or big pumps and holes, this change gets higher. So, it is concluded that from the aspects of accuracy and generality, it is better to consider the spring force as non-linear. This choice is more reasonable if the designer designs

the suspension for a wide range of usage, like in SUV vehicles.

Table 7.1: Effect of taking spring as linear on sprung mass acceleration RMS

Road Profile	Non-linear Spring	Linear Spring	Change %
Road Class B	0.4332	0.4292	-0.9250
Road class C	0.8627	0.8544	-0.9633
Road Class D	1.7239	1.7061	-1.0344
Road Class E	3.4519	3.4102	-1.2077

7.2 Sprung Mass Estimation

Using EKF parameter estimator, estimation of suspension static deflection for non-linear quarter car model considering three different values of sprung mass was done. As mentioned before, estimating static suspension deflection, means estimating sprung mass through equation 4.1.

Simulations results are presented in table 7.2. In this table, real and estimated values of d_{s0} are given. Also, the estimation time i.e. the time it takes for the estimator to output the $\hat{d}_{s0}$ is provided. It can be observed that, the estimated and the actual values are very close to each other with a maximum error of 0.6%. Furthermore, this is achieved in a short period of time; around $1\ (s)$ for the first two cases and around $2\ (s)$ for the third case.

In figures 7.1, 7.3 and 7.5 the simulation results for the estimation performance for each case are presented. The solid line is the real value, The dash dot red line is the output of the EKF block and the blue dashed line is the output of the estimator. Estimation error covariance i.e. P_{55} for each case is also provided in these figures. The point where P_{55} reaches the pre-defined threshold 1×10^{-5} for the first time is highlighted. This is the point where the first criteria explained in section 6.5 is satisfied.

Table 7.2: d_{s0} estimation results

Vehicle	$m_s(kg)$	$d_{s0}(m)$	$\hat{d}_{s0}(m)$	$t_{est}(s)$
Unloaded	1241.78	-0.15092	-0.1519	0.8530
Half-loaded	1444.59	-0.175	-0.1762	1.3330
Full-loaded	1657.08	-0.2	-0.2001	2.0850

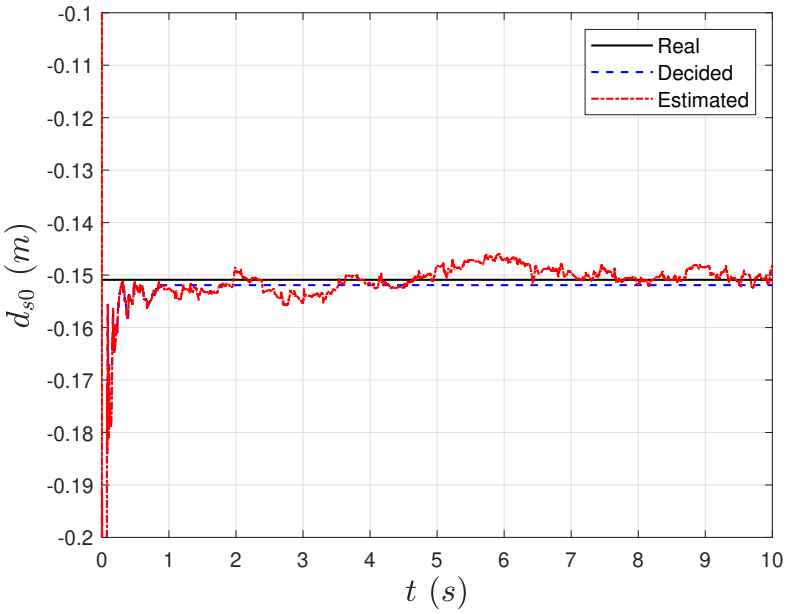

Figure 7.1: Comparison of real value of d_{s0} and its estimation versus time for unloaded vehicle

7.3 OSMC Performance

In this section, passive suspension, OSMC and IOSMC active suspensions are compared with each other with respect to three metrics: tire deflection, suspension deflection and sprung mass acceleration. This comparison along with the actuator force can be found in table 7.3 and figures 7.7 to figure 7.12. The sprung mass acceleration is ISO-2631 filtered. Both RMS and maximum values for tire and suspension deflection are provided.

OSMC improves suspension performance, compared to passive suspension, for all

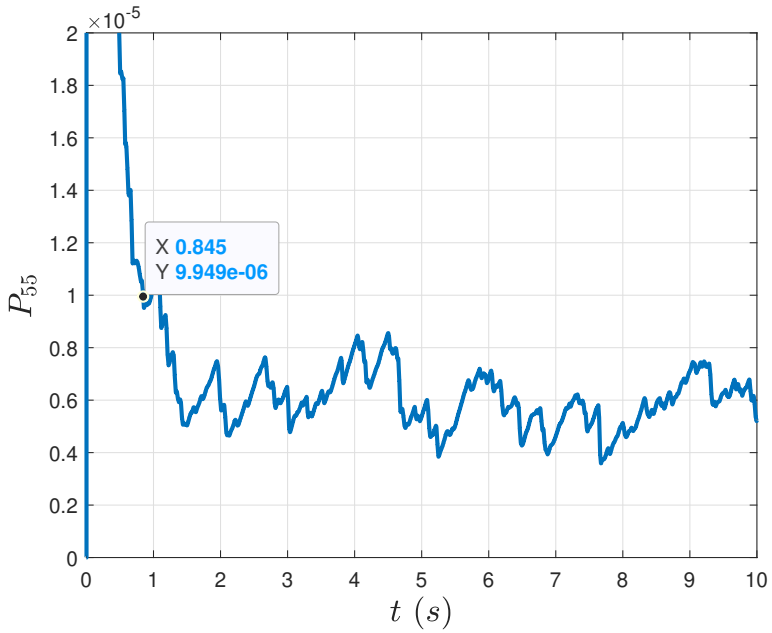

Figure 7.2: Estimation error covariance matrix $(5, 5)$ element value for unloaded vehicle

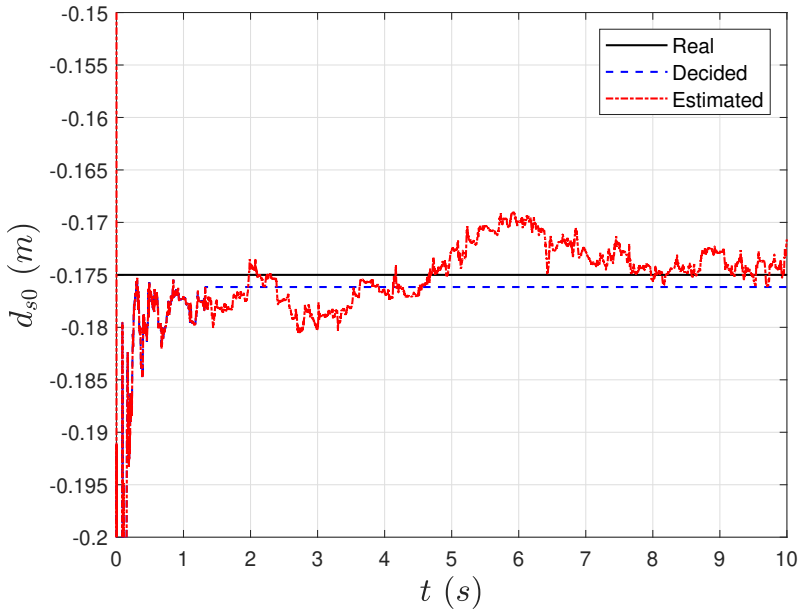

Figure 7.3: Comparison of real value of d_{s0} and its estimation versus time for half-loaded vehicle

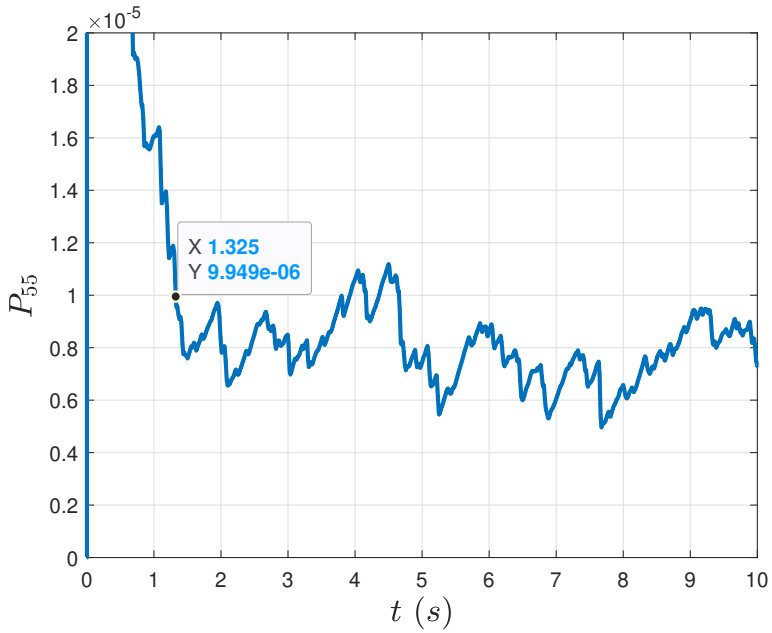

Figure 7.4: Estimation error covariance matrix $(5, 5)$ element value for half-loaded vehicle

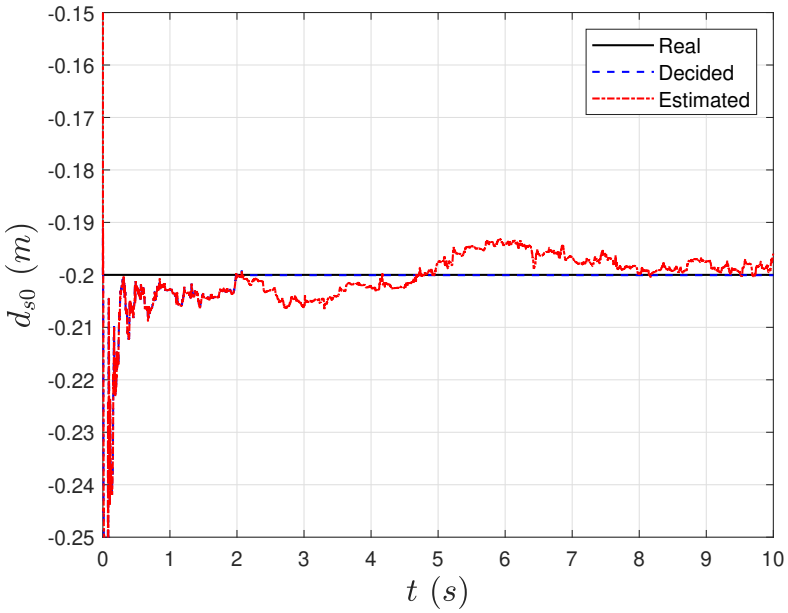

Figure 7.5: Comparison of real value of d_{s0} and its estimation versus time for full-loaded vehicle

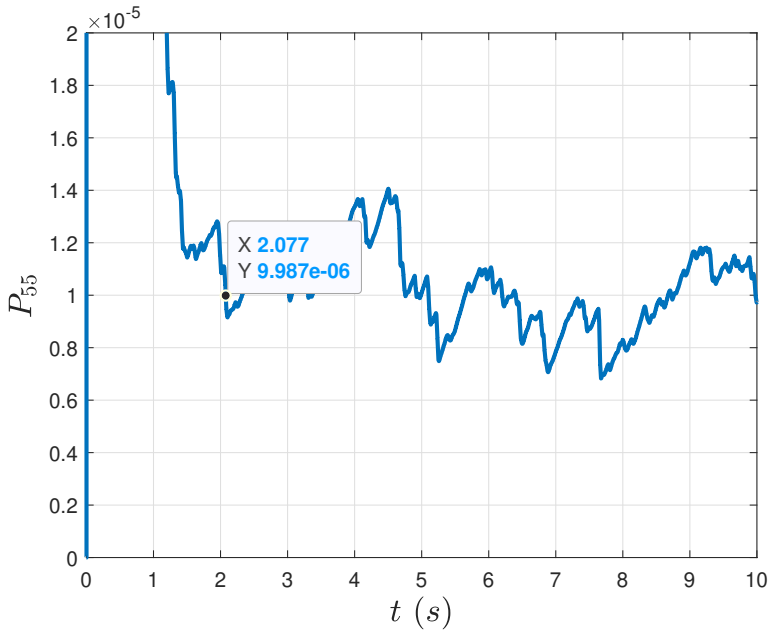

Figure 7.6: Estimation error covariance matrix $(5, 5)$ element value for full-loaded vehicle

the metrics. The improvement in sprung mass acceleration is 20.38%. Furthermore the improvement in tire deflection and suspension deflection are 2.95% and 8.18% respectively.

It is also observed that the RMS value of sprung mass acceleration is lower for OSMC compared to IOSMC, meaning that the former provides a better ride comfort than the latter [1]. RMS value of the sprung mass acceleration with OSMC is also around the comfort boundary with respect to table 6.7.

Figure 7.7 shows the performance of EKF state estimator described in section 5.8. The solid blue lines are the real states and red dashed lines are the estimated ones. As observed from this figure, the estimation performance is quite satisfactory.

When figures 7.8 and 7.9 are observed, it is seen that the trend with OSMC is lower compared to passive suspension, for tire and suspension deflection respectively.

Sprung mass acceleration also shows a lower trend with OSMC compared to passive

[1] The weighting factors used in [17] for IOSMC are considered here, they were not tuned to get a lower sprung mass acceleration

Table 7.3: Performance comparison of different suspensions

Parameter	Unit	Passive	OSMC	ISOMC
Sprung Mass Acceleration RMS	$\frac{m}{s^2}$	0.4332	0.3449	0.3917
Suspension Deflection RMS	mm	4.6000	4.5535	4.2136
Suspension Deflection Max	mm	11.5710	5.7753	17.2226
Tire Deflection RMS	mm	1.7269	1.6758	1.5045
Tire Deflection Max	mm	6.7566	6.5543	6.4645
Actuator Force RMS	N	0	347.6807	328.8790

suspension and IOSMC as observed in figure 7.10. Also PSD diagram of sprung mass acceleration is given in figure 7.11. Reduction of the sprung mass acceleration PSD, especially in the frequency range lower that 10 Hz is observed. As mentioned before, $3-9$ Hz is the critical frequency range regarding passenger ride comfort. Therefore, this result shows that OSMC is effective in improving ride comfort. Figure 7.12 shows actuator force of OSMC and IOSMC in time domain. Actuator force with OSMC is more oscillatory than IOSMC as expected since OSMC applies relay control where as IOSMC applies equivalent control.

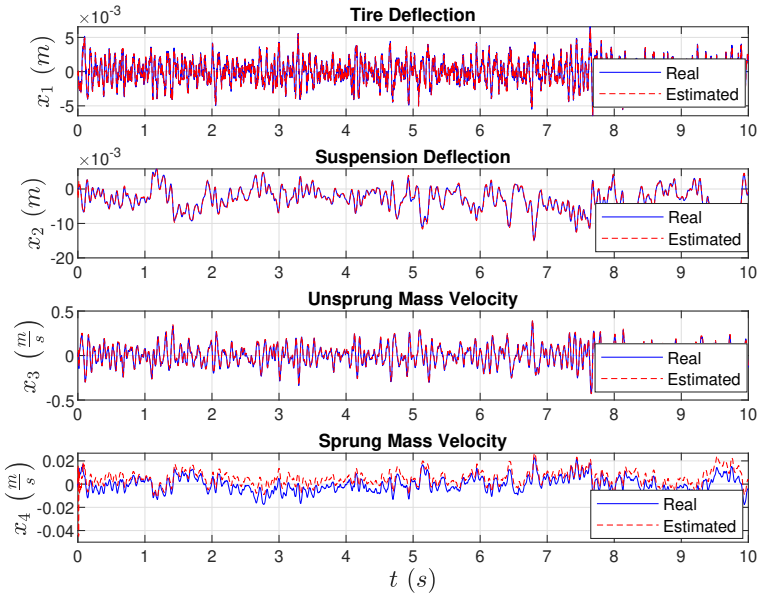

Figure 7.7: Estimated states vs real states

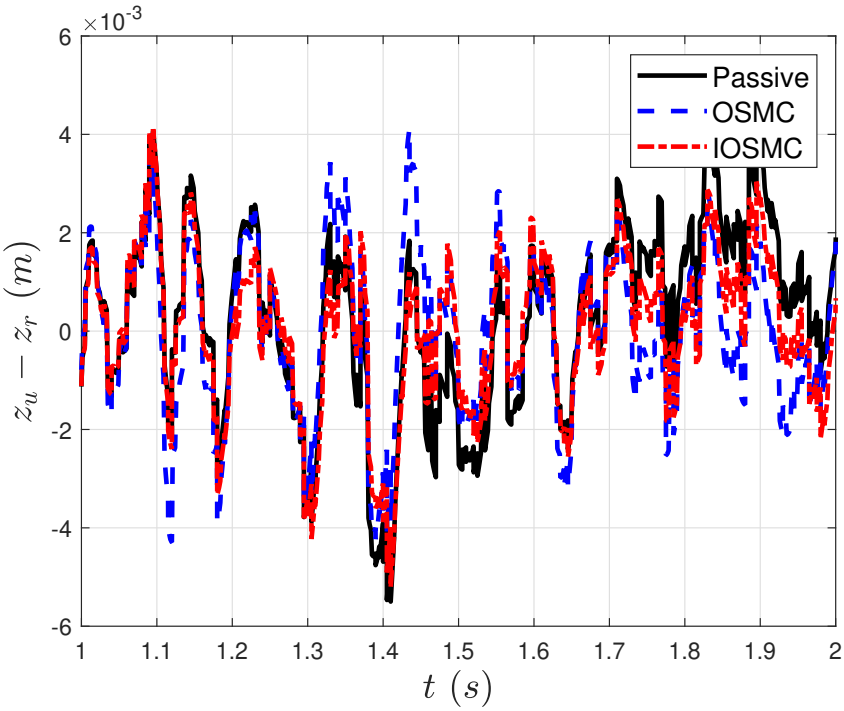

Figure 7.8: Tire deflection vs time for different suspensions

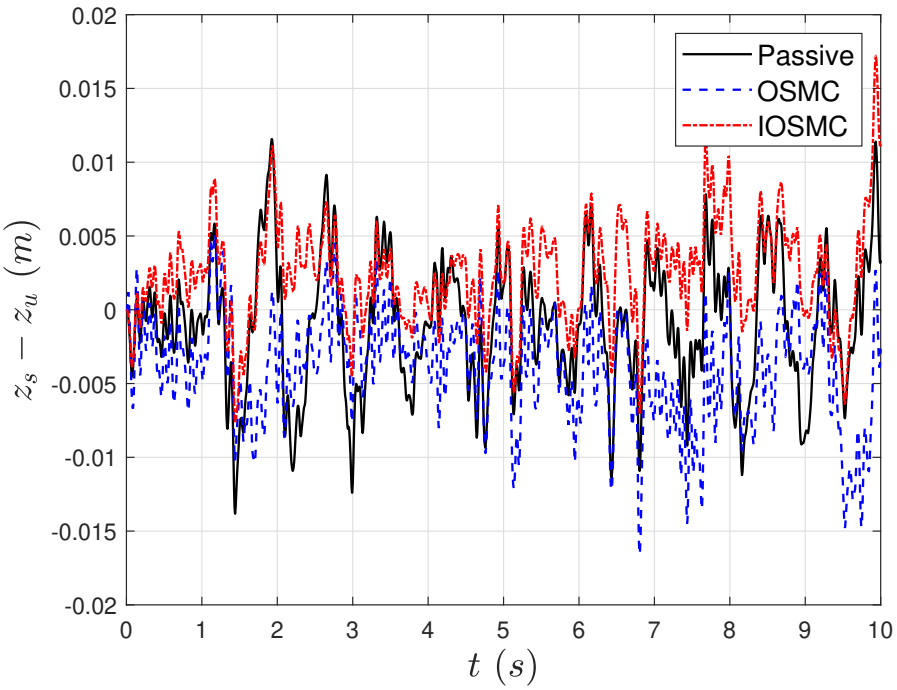

Figure 7.9: Suspension deflection vs time for different suspensions

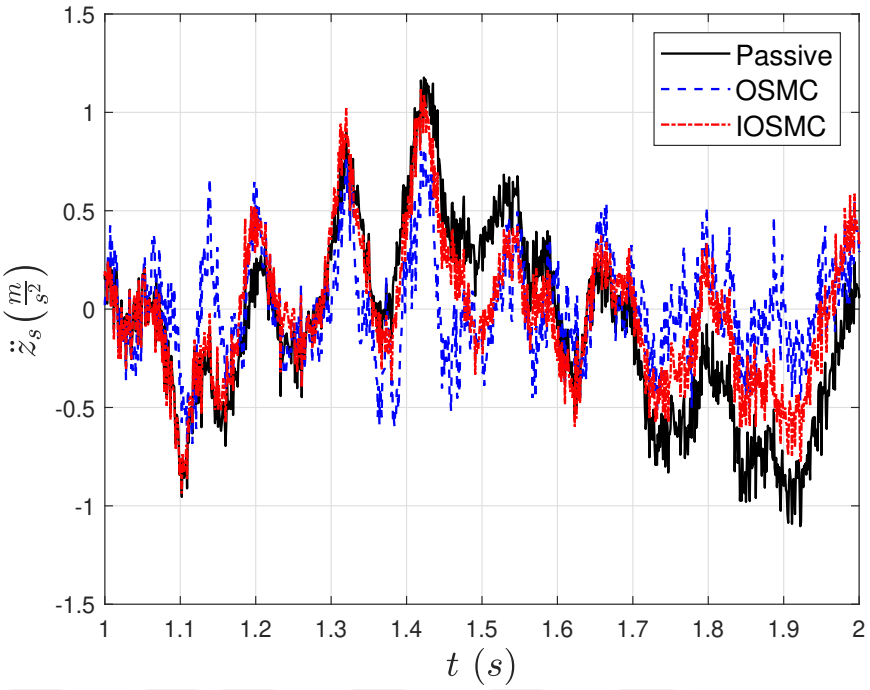

Figure 7.10: Sprung mass acceleration vs time for different suspensions

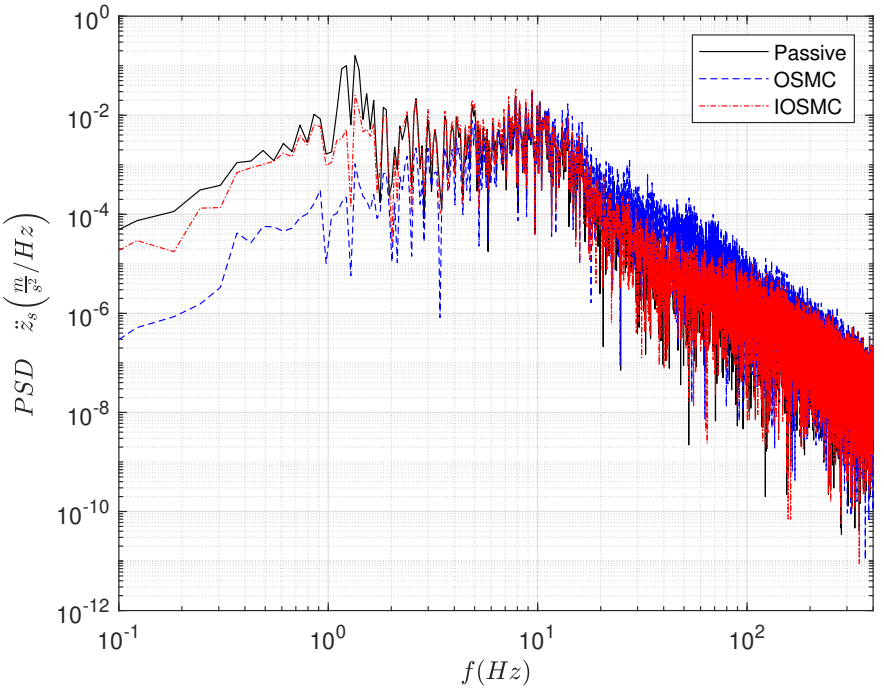

Figure 7.11: ISO-2631 filtered PSD of sprung mass acceleration

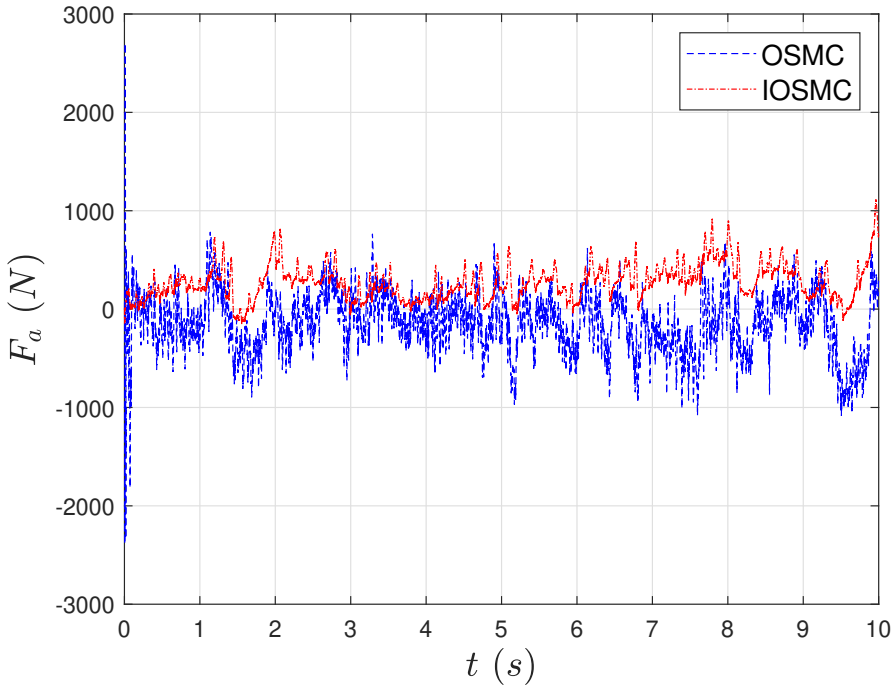

Figure 7.12: Actuator force vs time for different suspensions

7.4 Effect of Using Incorrect Sprung Mass In the Control Algorithm

As it was described in chapter 4, sprung mass is an uncertain parameters to the controller. The vehicle can be assumed to be fully loaded as the worst case scenario, half-loaded or even unloaded in the control algorithm. Based on these 3 scenarios, simulations are performed considering 9 different cases. Sprung mass acceleration RMS value which is metric for ride comfort, is provided in table 7.4 for these 9 cases.

Table 7.4: Sprung Mass Acceleration RMS $\left(\frac{m}{s^2}\right)$ for different cases of vehicle mass

Real \Controller	Unloaded	Half-loaded	Full-Loaded
Unloaded	0.3449	0.4358	0.4325
Half-Loaded	0.3195	0.3254	0.3854
Full-loaded	0.2911	0.2982	0.3083

Rows indicate the loading configuration of the vehicle, whereas the columns indicate

the controller configuration. Based on the results give in the table 7.4, for an unloaded vehicle, sprung mass acceleration RMS increases for the second and the third cases respectively, compared to the first case. The reason of this is explained by using table 7.5. In this table, it is shown that using a higher sprung mass value in the control algorithm compared to the actual one, has a similar effect to reducing the weight of sprung mass speed within the OSMC. It can be observed that, the eigenvalues of the sliding mode motion, when this weighting factor is reduced by half are almost the same as the case where the sprung mass information is higher than the actual one.

Table 7.5: Effect of using higher d_{s0} on eigenvalues

Weighting Factors	d_{s0}	$\hat{d}_{s0}$	Eigenvalues
$\delta_1 = 35689$ $\delta_2 = 27862$ $\delta_3 = 10000$	-0.1509	-0.1519	$-1.6838 + 0.0000i$ $-15.7499 \pm 61.3728i$
$\delta_1 = 35689$ $\delta_2 = 27862$ $\delta_3 = \frac{10000}{2}$	-0.1509	-0.1519	$-2.4030 + 0.0000i$ $-22.2621 \pm 59.0151i$
$\delta_1 = 35689$ $\delta_2 = 27862$ $\delta_3 = 10000$	-0.1509	-0.2001	$-1.6888 + 0.0000i$ $-20.8871 \pm 59.7216i$

This behavior is observed from the second row as well. Considering a fully-loaded vehicle configuration in control design where the vehicle is actually half-loaded, results in an increase in sprung mass acceleration RMS value. On the other hand, considering a half-loaded or unloaded vehicle configuration in control design, results in a decrease in sprung mass acceleration RMS value.

In regard to these results, it may be concluded that taking a low value for d_{s0} within the control algorithm (regardless of the real value) would yield a lower sprung mass acceleration. However, in such a case, the sliding surface coefficients; i.e. the desired Eigenvalues are computed incorrect, again. Table 7.6 shows the effect of taking a lower d_{s0} value within the control algorithm, on the Eigenvalues.

Again, with incorrect d_{s0} information, shown by the third case of Table 7.6, the Eigenvalues reduce compared to the first case where the d_{s0} information is correct. There is a similar effect on the Eigenvalues when the weighting of the suspension deflection, δ_2, is reduced, as shown by the second case of Table 7.6. Therefore, it may be concluded that using a lower d_{s0} in the control algorithm, compared to the actual one, would generate a tendency towards undesired suspension deflection increase. This prediction has been checked with simulations. The RMS value for the suspension deflection increased 2.67 times, when the actual d_{s0} is $-0.2\ (m)$ but the one used in the controller is $-0.15(m)$, despite a reduction in sprung mass acceleration.

Table 7.6: Effect of using lower d_{s0} on eigenvalues

Weighting Factors	d_{s0}	$\hat{d}_{s0}$	Eigenvalues
$\delta_1 = 35689$ $\delta_2 = 27862$ $\delta_3 = 10000$	-0.2	-0.2001	$-1.6888 + 0.0000i$ $-20.8871 \pm 59.7216i$
$\delta_1 = 35689$ $\delta_2 = \frac{27862}{2}$ $\delta_3 = 10000$	-0.2	-0.2001	$-1.18715 + 0.0000i$ $-18.4616 \pm 60.7105i$
$\delta_1 = 35689$ $\delta_2 = 27862$ $\delta_3 = 10000$	-0.2	-0.1519	$-1.6838 + 0.0000i$ $-15.7499 \pm 61.3728i$

The discussion above, about the effect of using incorrect sprung mass information within the control algorithm, was based on incorrect calculation of optimal sliding surface coefficients.

There are two other reasons why using incorrect sprung mass information deteriorates the controller performance. The first one is state estimation. When the sprung mass information is incorrect, EKF state estimator uses an incorrect value. The results of such an incorrect estimation are shown in figure 7.13. It is observed from this figure that, there is an estimation offset for the sprung mass speed when the sprung mass information used by the controller ($\hat{d}_{s0} = -0.1519\ (m)$) was higher than the actual one ($d_{s0} = -0.2\ (m)$)

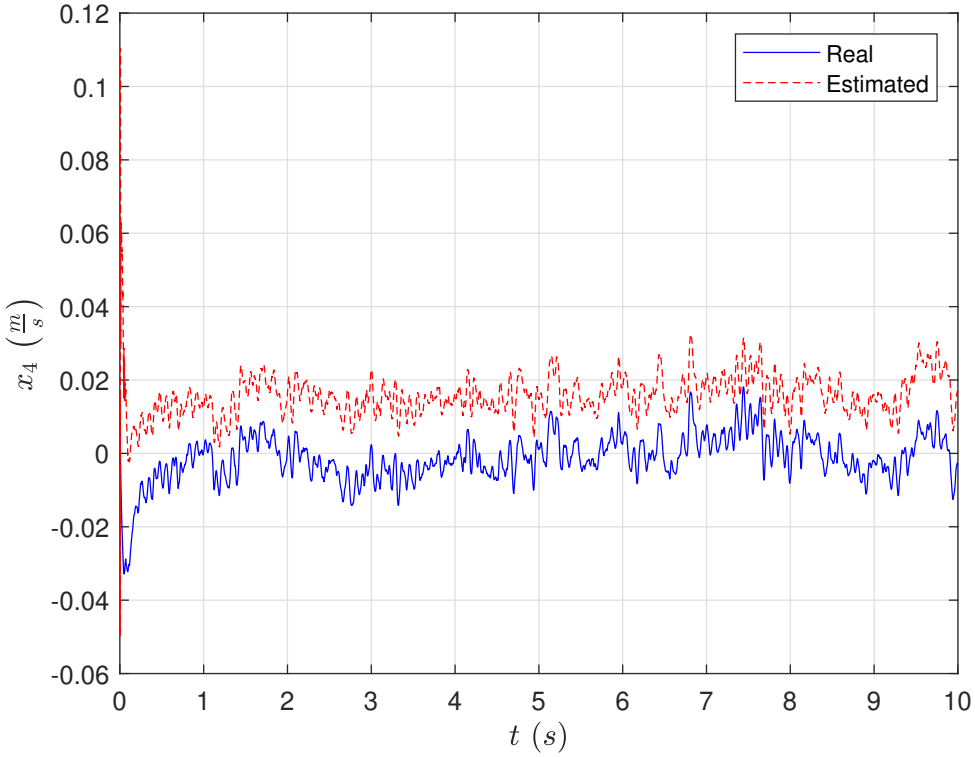

Figure 7.13: Effect of using incorrect sprung mass on estimated states

The second one is the de-linearization step in the controller design. As observed from equation 5.53, incorrect sprung mass information yields an incorrect controller gain. If the non-linear control input F_a, given by equation 5.53 is substituted in sprung mass acceleration given by equation 3.32 and considering that the state estimation errors are negligible, the following equation is obtained:

$$\dot{x}_4 = \frac{gk_{2s}\Big(3x_2^2(\hat{d}_{s0} - d_{s0}) + 3x_2(\hat{d}_{s0}^2 - d_{s0}^2)\Big)}{-k_{1s}d_{s0} - k_{2s}d_{s0}^3} + \frac{k_{1s}\hat{d}_{s0} + k_{2s}\hat{d}_{s0}^3}{k_{1s}d_{s0} + k_{2s}d_{s0}^3}\big[-U\tanh 3S\big] \tag{7.2}$$

The first term in equation 7.2 has a range of $[-0.02 \quad 0]$ which is negligible compared to sprung mass acceleration range of $[-1.5 \quad 1.5]$. On the other hand, the sliding mode controller gain U would change in an undesired way, when $\hat{d}_{s0}$ and d_{s0} are different. This change is tabulated and shown in table 7.7. Rows correspond to the real situation of the vehicle and columns correspond to configuration considered in control design. The change in controller gain is around -24% for a full-loaded vehicle with unloaded configuration considered in control design. On the other hand, for the opposite case,

i.e. considering full-loaded vehicle configuration for an unloaded vehicle results in a 33% increase in controller gain U.

Table 7.7: Percent change in control gain U for different cases of vehicle mass

Real \Controller	Unloaded	Half-loaded	Full-Loaded
Unloaded	0.6747	17.1491	33.5120
Half-Loaded	-13.4590	0.7024	14.7682
Full-loaded	-24.5561	-12.2105	0.05157

It should be noted that these undesired changes due to incorrect sprung mass information can be compensated by picking the controller gain U accordingly, from a stability standpoint. For instance, increasing the controller gain for providing stability is one alternative. The other alternative is (which is one of the main claims in this work) estimating sprung mass and using the nominal controller gain. By means, the undesired increase in sprung mass acceleration can be avoided.

The three reasons given above state why correct sprung mass information would improve the performance of the sliding mode control.

7.5 Conclusion

In this study an optimal sliding mode controller was designed for a non-linear quarter car model suspension. The road profile was modeled considering ISO-8608 and sprung mass acceleration was filtered according to ISO-2631 standard. The OSMC was compared to passive suspension and another version of sliding mode control proposed by [17]. Lastly, the effect of using incorrect sprung mass information within the control algorithm was investigated. Simulation results show that:

- The OSMC developed in this work, reduces sprung mass acceleration, therefore improves ride comfort. Also, the simulation results show that the suspension deflection and tire deflection, are lower compared to the case of passive suspension.

- The OSMC yields a lower sprung mass acceleration compared to IOSMC. Also, the maximum suspension deflection is lower than that of IOSMC.
- using incorrect sprung mass information in the control algorithm ends up with the following undesired results:
    1. Errors in the state estimation.
    2. Incorrect calculation of the controller gain during the de-linearization stage of the controller, which may end up with an undesired increase in sprung mass acceleration.
    3. Designing the controller, considering unloaded vehicle configuration, ends up with an undesired increase in sprung mass acceleration for the half-loaded and full-loaded vehicle configurations.
    4. Designing the controller for a full-loaded vehicle configuration would end up with an undesired increase in suspension deflection, for unloaded or half-loaded vehicle configurations.

7.6 Future Work

The following suggestions are considered as the future work to be done:

- Investigating the performance of OSMC for a half-car model and controlling sprung mass and pitch accelerations simultaneously.
- Estimation of tire stiffness which is also subject to change during the drive cycle of the vehicle.

REFERENCES

[1] I. ISO, "Mechanical vibration and shock–evaluation of human exposure to wholebody vibrations (2631-1)," *International Standards Organization*, 1997.

[2] N. Reza, "Jazar. vehicle dynamics: Theory and application.-springer science," 2008.

[3] S. M. Savaresi, C. Poussot-Vassal, C. Spelta, O. Sename, and L. Dugard, *Semi-active suspension control design for vehicles*. Elsevier, 2010.

[4] H. Liu, H. Gao, and P. Li, *Handbook of vehicle suspension control systems*. Institution of Engineering and Technology, 2013.

[5] Y. Savas and H. I. Basturk, "Adaptive backstepping control design for active suspension systems actuated by four-way valve-piston," in *Proceedings of the American Control Conference*, pp. 438–443, Institute of Electrical and Electronics Engineers Inc., jun 2017.

[6] W. Bauer, *Hydropneumatic suspension systems*. Springer Science & Business Media, 2010.

[7] B. L. Gysen, J. L. Janssen, J. J. Paulides, and E. A. Lomonova, "Design aspects of an active electromagnetic suspension system for automotive applications," *IEEE transactions on industry applications*, vol. 45, no. 5, pp. 1589–1597, 2009.

[8] B. Gysen, *Generalized harmonic modeling technique for 2D electromagnetic problems*. No. december, 2011.

[9] M. Münster, U. Mair, H.-J. Gilsdorf, A. Thomä, C. Müller, M. Hippe, and J. Hoffmann, "Electromechanical active body control," *ATZautotechnology*, vol. 9, no. 3, pp. 24–29, 2009.

[10] W. Evers, "Improving driver comfort in commercial vehicles: Modeling and control of a low-power active cabin suspension system," *Eindhoven, The Netherlands: Eindhoven University of Technology*, 2010.

[11] W.-J. Evers, A. Teerhuis, A. van der Knaap, I. Besselink, and H. Nijmeijer, "The electromechanical low-power active suspension: Modeling, control, and prototype testing," *Journal of dynamic systems, measurement, and control*, vol. 133, no. 4, 2011.

[12] K. Sharma, D. Crolla, and D. Wilson, "The design of a fully active suspension system incorporating a kalman filter for state estimation," in *1994 International Conference on Control-Control'94.*, vol. 1, pp. 344–349, IET, 1994.

[13] D. Hrovat, "Applications of optimal control to advanced automotive suspension design," 1993.

[14] Bose, "Active suspension system," *http://www.bose.com*, 2004.

[15] T. DRIVE, "The crazy bose 'magic carpet' car suspension system is finally headed for production." `https://bit.ly/2DEzavg`, 2020.

[16] S. Bououden, M. Chadli, and H. R. Karimi, "A Robust Predictive Control Design for Nonlinear Active Suspension Systems," *Asian Journal of Control*, vol. 18, no. 1, pp. 122–132, 2016.

[17] S. A. Chen, J. C. Wang, M. Yao, and Y. B. Kim, "Improved optimal sliding mode control for a non-linear vehicle active suspension system," *Journal of Sound and Vibration*, vol. 395, pp. 1–25, may 2017.

[18] A. G. Mohite and A. C. Mitra, "Development of Linear and Non-linear Vehicle Suspension Model," in *Materials Today: Proceedings*, vol. 5, pp. 4317–4326, Elsevier Ltd, jan 2018.

[19] T. T. Tran, "Feedback linearization and backstepping: an equivalence in control design of strict-feedback form," *IMA Journal of Mathematical Control and Information*, 2019.

[20] D. Hrovat, "Survey of advanced suspension developments and related optimal control applications," *Automatica*, vol. 33, no. 10, pp. 1781–1817, 1997.

[21] T. Schwarzgruber, E. Grünbacher, and L. Del Re, "Performance oriented tuning approach for a nonlinear controlled active suspension system," *IFAC Proceedings Volumes (IFAC-PapersOnline)*, vol. 43, no. 14, pp. 891–896, 2010.

[22] B. L. Gysen, T. P. Van Der Sande, J. J. Paulides, and E. A. Lomonova, "Efficiency of a regenerative direct-drive electromagnetic active suspension," *IEEE Transactions on Vehicular Technology*, vol. 60, no. 4, pp. 1384–1393, 2011.

[23] L. X. Guo and L. P. Zhang, "Robust $H\infty$ control of active vehicle suspension under non-stationary running," *Journal of Sound and Vibration*, vol. 331, pp. 5824–5837, dec 2012.

[24] R. Wang, H. Jing, H. R. Karimi, and N. Chen, "Robust fault-tolerant H_∞ control of active suspension systems with finite-frequency constraint," *Mechanical Systems and Signal Processing*, vol. 62, pp. 341–355, 2015.

[25] H. Li, Z. Zhang, H. Yan, and X. Xie, "Adaptive Event-Triggered Fuzzy Control for Uncertain Active Suspension Systems," *IEEE Transactions on Cybernetics*, sep 2018.

[26] V. S. Deshpande, B. Mohan, P. Shendge, and S. Phadke, "Disturbance observer based sliding mode control of active suspension systems," *Journal of Sound and Vibration*, vol. 333, no. 11, pp. 2281–2296, 2014.

[27] H. Pan, W. Sun, H. Gao, and J. Yu, "Finite-Time Stabilization for Vehicle Active Suspension Systems with Hard Constraints," *IEEE Transactions on Intelligent Transportation Systems*, vol. 16, no. 5, pp. 2663–2672, 2015.

[28] Y. Huang, J. Na, X. Wu, X. Liu, and Y. Guo, "Adaptive control of nonlinear uncertain active suspension systems with prescribed performance," *ISA transactions*, vol. 54, pp. 145–155, 2015.

[29] S. Bououden, M. Chadli, and H. R. Karimi, "A Robust Predictive Control Design for Nonlinear Active Suspension Systems," *Asian Journal of Control*, vol. 18, no. 1, pp. 122–132, 2016.

[30] J. J. Rath, M. Defoort, H. R. Karimi, and K. C. Veluvolu, "Output Feedback Active Suspension Control with Higher Order Terminal Sliding Mode," *IEEE Transactions on Industrial Electronics*, vol. 64, pp. 1392–1403, feb 2017.

[31] S. Wen, M. Z. Chen, Z. Zeng, X. Yu, and T. Huang, "Fuzzy Control for Uncertain Vehicle Active Suspension Systems via Dynamic Sliding-Mode Approach,"

IEEE Transactions on Systems, Man, and Cybernetics: Systems, vol. 47, pp. 24–32, jan 2017.

[32] D. Wang, D. Zhao, M. Gong, and B. Yang, "Nonlinear Predictive Sliding Mode Control for Active Suspension System," *Shock and Vibration*, vol. 2018, pp. 1–10, 2018.

[33] H. Pang, X. Zhang, J. Yang, and Y. Shang, "Adaptive backstepping-based control design for uncertain nonlinear active suspension system with input delay," *International Journal of Robust and Nonlinear Control*, vol. 29, pp. 5781–5800, aug 2019.

[34] J. Mrazgua, E. H. Tisssir, and M. Ouahi, "Fuzzy Fault-Tolerant H_∞ Control Approach for Nonlinear Active Suspension Systems with Actuator Failure," *Procedia Computer Science*, vol. 148, pp. 465–474, 2019.

[35] B. Lin and X. Su, "Fault-tolerant Controller Design for Active Suspension System with Proportional Differential Sliding Mode Observer," *International Journal of Control, Automation and Systems*, vol. 17, no. 7, pp. 1751–1761, 2019.

[36] V. Utkin, "Sliding modes in control and optimization springer-verlag," *New York*, 1992.

[37] B. L. Zhang, G. Y. Tang, and F. L. Cao, "Optimal sliding mode control for active suspension systems," in *Proceedings of the 2009 IEEE International Conference on Networking, Sensing and Control, ICNSC 2009*, pp. 351–356, 2009.

[38] C. Zhou, X. Liu, W. Chen, F. Xu, and B. Cao, "Optimal sliding mode control for an active suspension system based on a genetic algorithm," *Algorithms*, vol. 11, dec 2018.

[39] H. Pang, Y. Wang, X. Zhang, and Z. Xu, "Robust state-feedback control design for active suspension system with time-varying input delay and wheelbase preview information," *Journal of the Franklin Institute*, vol. 356, pp. 1899–1923, mar 2019.

[40] H. Pang, X. Zhang, J. Chen, and K. Liu, "Design of a coordinated adaptive backstepping tracking control for nonlinear uncertain active suspension system," *Applied Mathematical Modelling*, vol. 76, pp. 479–494, 2019.

[41] H. Pang, X. Zhang, and Z. Xu, "Adaptive backstepping-based tracking control design for nonlinear active suspension system with parameter uncertainties and safety constraints," *ISA Transactions*, vol. 88, pp. 23–36, 2019.

[42] W. Gang, "ESO-Based Terminal Sliding Mode Control for Uncertain Full-Car Active Suspension Systems," *International Journal of Automotive Technology*, vol. 21, pp. 691–702, jun 2020.

[43] M. Du, D. Zhao, M. Yang, and H. Chen, "Nonlinear extended state observer-based output feedback stabilization control for uncertain nonlinear half-car active suspension systems," *Nonlinear Dynamics*, may 2020.

[44] G. Koch, T. Kloiber, and B. Lohmann, "Nonlinear and filter based estimation for vehicle suspension control," in *Proceedings of the IEEE Conference on Decision and Control*, pp. 5592–5597, 2010.

[45] G. Koch, T. Kloiber, E. Pellegrini, and B. Lohmann, "A nonlinear estimator concept for active vehicle suspension control," in *Proceedings of the 2010 American Control Conference*, pp. 4576–4581, IEEE, 2010.

[46] W. Chen, H. Xiao, Q. Wang, L. Zhao, and M. Zhu, *Integrated vehicle dynamics and control*. John Wiley & Sons, 2016.

[47] J. C. Dixon, *The shock absorber handbook*. John Wiley & Sons, 2008.

[48] J. K. Hedrick and A. Girard, "Control of nonlinear dynamic systems: Theory and applications," *Controllability and observability of Nonlinear Systems*, p. 48, 2005.

[49] M. S. Grewal and A. P. Andrews, *Kalman filtering: Theory and Practice with MATLAB*. John Wiley & Sons, 2014.

[50] Y. Bar-Shalom, X. R. Li, and T. Kirubarajan, *Estimation with applications to tracking and navigation: theory algorithms and software*. John Wiley & Sons, 2004.

[51] R. DeCarlo and S. Zak, "A quick introduction to sliding mode control and its applications." `https://bit.ly/2DEzmL0`, 2008.

[52] A. Isidori, “Non-linear control systems: an introduction, 1995.”

[53] J. P. Calvet and Y. Arkun, “Feedforward and feedback linearization of non-linear systems with disturbances,” *International Journal of Control*, vol. 48, no. 4, pp. 1551–1559, 1988.

[54] K. Ogata and Y. Yang, *Modern control engineering*, vol. 5. Prentice hall Upper Saddle River, NJ, 2010.

[55] V. Utkin, J. Guldner, and M. Shijun, *Sliding mode control in electro-mechanical systems*, vol. 34. CRC press, 1999.

[56] O. Gerger, “Design, control and optimization of vehicle suspensions with inerters,” Master’s thesis, Middle East Technical University, Turkey, Ankara, 2013.

[57] ISO-8608, “International Standard 8608: Mechanical Vibration – Road Surface Profiles – Reporting of Measured Data,” vol. 2016, p. 29, 2011.

[58] C. S. Dharankar, M. K. Hada, and S. Chandel, “Numerical generation of road profile through spectral description for simulation of vehicle suspension,” *Journal of the Brazilian Society of Mechanical Sciences and Engineering*, vol. 39, no. 6, pp. 1957–1967, 2017.

[59] F. Tyan, Y.-F. Hong, S.-H. Tu, and W. S. Jeng, “Generation of random road profiles,” *Journal of Advanced Engineering*, vol. 4, no. 2, pp. 151–156, 2009.

[60] D. E. D. E. Newland, *An introduction to random vibrations, spectral and wavelet analysis*. Longman Scientific & Technical, 3rd ed., 1993.

Appendix A

SIMULINK MODELS OF QUARTER CAR MODELS

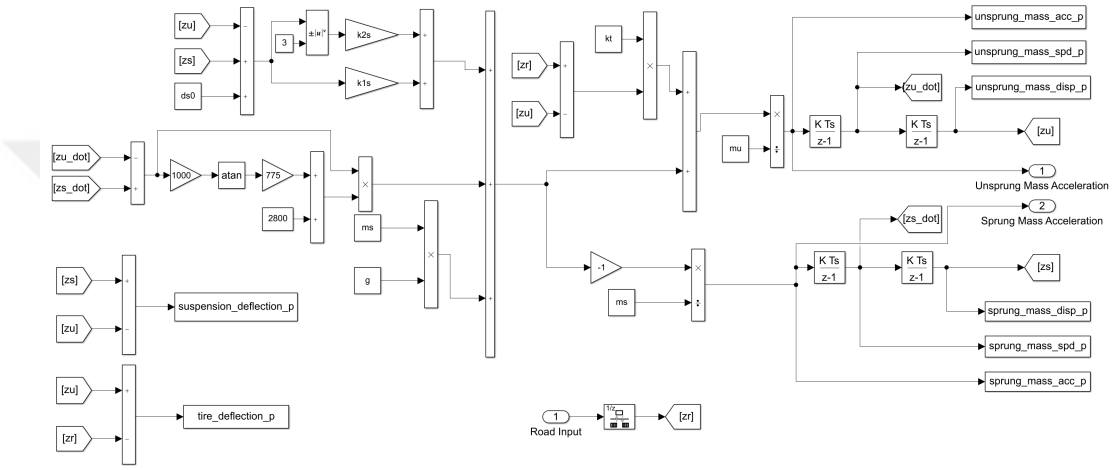

Figure A.1: Passive suspension sub-system detail

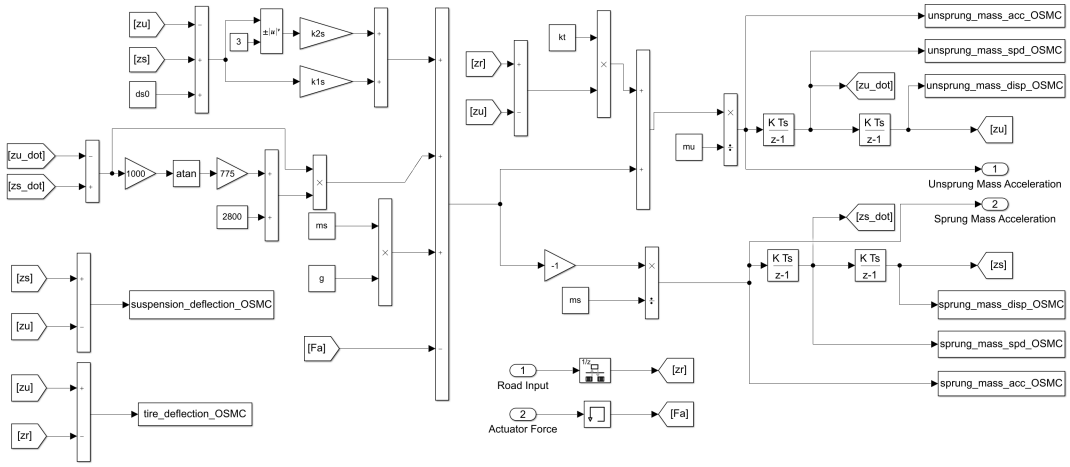

Figure A.2: Active suspension sub-system detail

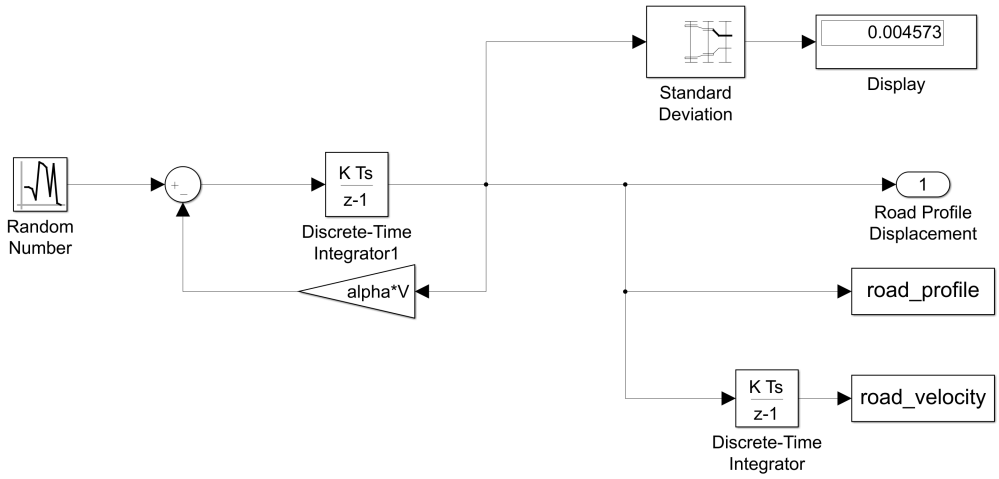

Figure A.3: Road profile generator sub-sytem detail

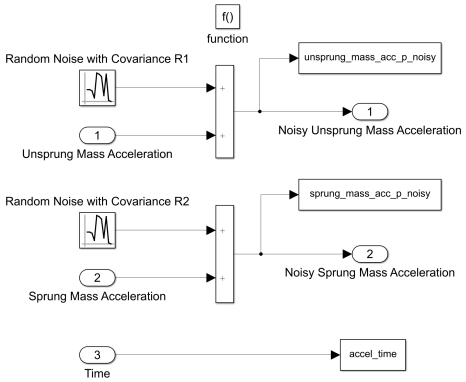

Figure A.4: Accelerometers sub-system detail

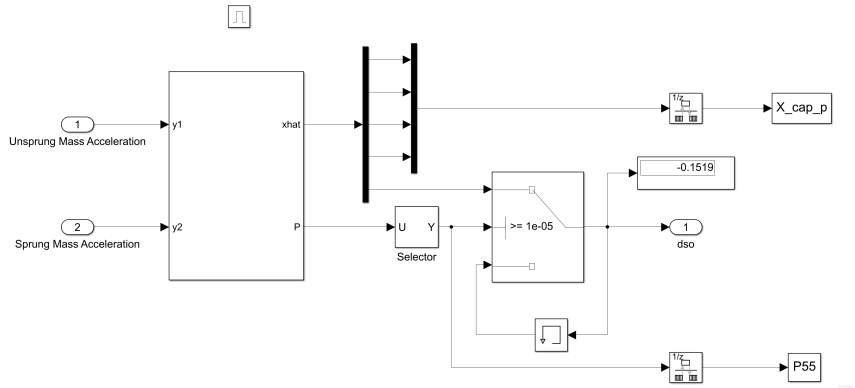

Figure A.5: Parameter estimator sub-system detail

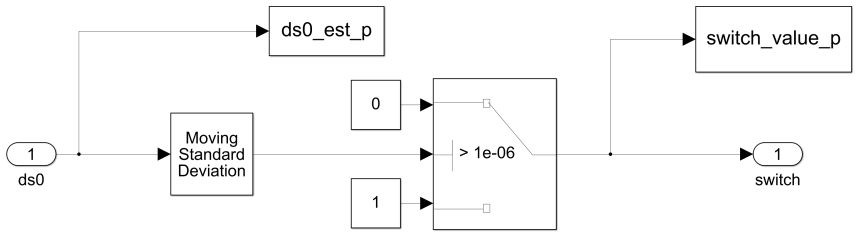

Figure A.6: Parameter estimator stopper sub-system detail

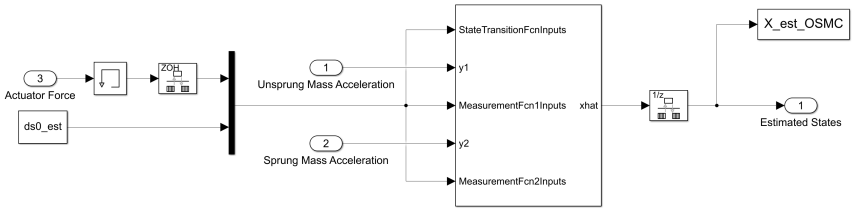

Figure A.7: State estimator sub-system detail

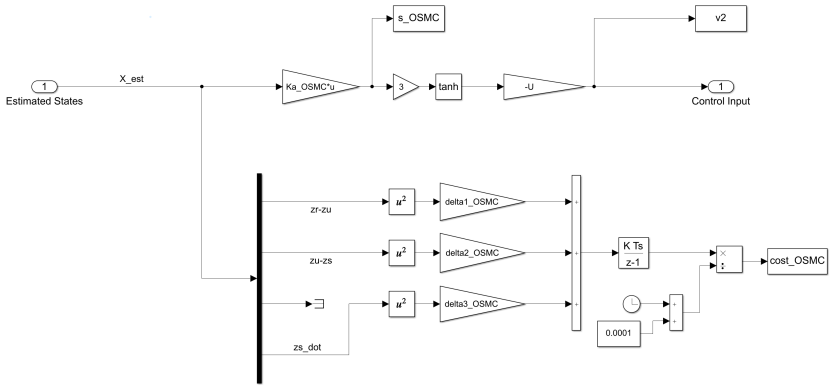

Figure A.8: OSMC controller sub-system detail

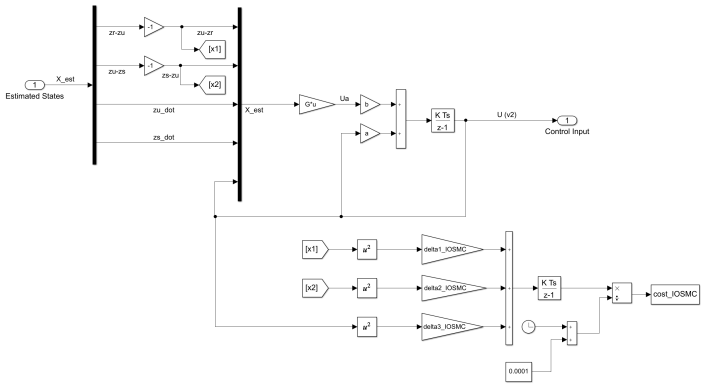

Figure A.9: IOSMC controller sub-system detail

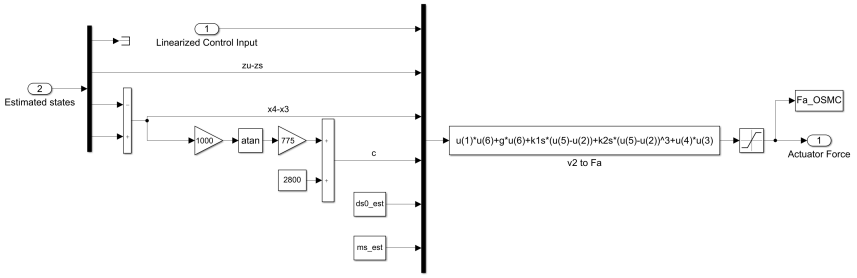

Figure A.10: De-linearization sub-system detail

Appendix B

ISO-2631 FILTER FOR SPRUNG MASS ACCELERATION [1]

This filter is a combination of four filters. In this section, the equations defining these filters and the associated filter parameters are provided.

The first filter is a high pass filter with the following frequency response function:

$$|H_h(f)| = \sqrt{\frac{f^4}{f^4 + f_1^4}} \tag{B.1}$$

where f_1 is the corner frequency.

Second one is a low pass filer with frequency response function of:

$$|H_l(f)| = \sqrt{\frac{f^4}{f^4 + f_2^4}} \tag{B.2}$$

where f_2 is the corner frequency. The product $|H_h(f)|.|H_l(f)|$ represents the band-limiting filter transfer function. The third filter is proportional to acceleration in low frequencies and proportional to speed at high frequencies.

$$|H_t(f)| = \sqrt{\frac{f^2 + f_3^2}{f_3^2}} . \sqrt{\frac{f^4 Q_4^2}{f^4 Q_4^2 + f^2 F_4^2 \left(1 - 2Q_4^2\right) + f_4^4 . Q_4^2}} \tag{B.3}$$

The last filter is proportional to jerk. Its frequency response function is:

$$|H_s(f)| = \frac{Q_6}{Q_5} \sqrt{\frac{f^4 Q_5^2 + f^2 f_5^2 \left(1 - 2Q_5^2\right) + f_5^4 Q_5^2}{f^4 Q_6^2 + f^2 f_6^2 \left(1 - 2Q_6^2\right) + f_6^4 Q_6^2}} \tag{B.4}$$

The product $|H_t(f)|.|H_s(f)|$ represents the actual weighting frequency response function. The total frequency response function of the filters is the product of four FRFs described above:

$$|H(f)| = |H_h(f)|.|H_l(f)|.|H_t(f)|.|H_s(f)| \tag{B.5}$$

Parameter	Value	Unit
f_1	0.4	Hz
f_2	100	Hz
f_3	12.5	Hz
f_4	12.5	Hz
f_5	2.37	Hz
f_6	3.35	Hz
Q_4	0.63	-
Q_5	0.91	-
Q_6	0.91	-

Table B.1: Parameters of the transfer functions of frequency weightings

The parameters of this filter, are provided in table B.1.

This filter is used for evaluating the RMS value of the sprung mass acceleration. The PSD os sprung mass acceleration is filtered by this filter. Then, area under the PSD curve i.e. the integral given below, is computed [60].

$$\ddot{z}_s^2 = 2\int_0^\infty S(f)\, df \tag{B.6}$$

$$\ddot{z}_{s,RMS} = \sqrt{\ddot{z}_s^2} \tag{B.7}$$

By means, the ISO-2631 filter sprung mass acceleration RMS value is obtained.